CINTAL - Centro de Investigação Tecnológica do Algarve

Universidade do Algarve

Tracking a cold filament with matched-field inversion

V. Corré

Rep 01/02 - SiPLAB
09/July/2002

University of Algarve
Campus da Penha
8000, Faro,
Portugal

tel: +351-289800131
fax: +351-289864258
cintal@ualg.pt
www.ualg.pt/cintal

Work requested by	CINTAL Universidade do Algarve, Campus da Penha, 8000 Faro, Portugal tel: +351-289800131, cintal@ualg.pt, www.ualg.pt/cintal
Laboratory performing the work	SiPLAB - Signal Processing Laboratory Universidade do Algarve, FCT, Campus de Gambelas, 8000 Faro, Portugal tel: +351-289800949, info@siplab.uceh.ualg.pt, www.ualg.pt/uceh/adeec/siplab
Projects	ATOMS - FCT, PDCTM/P/MAR/15296/1999
Title	Tracking a cold filament with matched-field inversion
Authors	V. Corré
Date	July 09, 2002
Reference	01/02 - SiPLAB
Number of pages	44 (forty four)
Abstract	Simulation tests are carried out to estimate the time, range and depth variations of ocean acoustic properties. The estimation is based on matched-field inversion defined by a coupled mode acoustic model, a linear misfit function and an hybrid search algorithm. It is shown that tracking cold filaments is possible even in non-optimal conditions.
Clearance level	UNCLASSIFIED
Distribution list	SiPLAB (1), CINTAL (2), FCT (1)
Total number of copies	4 (four)

intentionally blank

Contents

List of Figures

Chapter 1

Introduction

ATOMS is an ambitious project that aims at developing a monitoring system for the Portuguese EEZ using acoustic tomography. A preliminary test for this system is to monitor the recurrent cold filaments/upwellings that develop off of the south west coast of Portugal, using a single vertical array of receivers and a towed source. This paper presents a synthetic study that simulates the monitoring conditions of this particular region and intends to check the feasibility and limits of such a monitoring.

The estimation of range-dependent properties with a single array-source pair is a problem which solution may not be unique. Being aware that this difficulty is particularly true when data are contaminated with noise (i.e., in all real cases), our objective was to obtain a variability trend rather than very accurate estimates of the properties. In other words, detection and global tracking of the filaments were of prime interest rather than detailed mapping of the sea-temperature (or sound-speed) field.

While acoustic travel-time tomography [1] is now a well-developed technique for large-scale, deep-ocean regions, it is less adapted for studying filaments which are mesoscale features that develop in relatively shallow (400 m) areas. Using matched-field processing to estimate ocean sound speed [2, 3] is a more recent approach than tomography. However this approach has already shown good results and can treat any type of environment equally. It is therefore the approach adopted in this study.

This report is organised as follows. The waveguide model chosen to represent the range-dependent environment and the model parameters are defined in the next Section. Section 3 describes the matched-field inversion (MFI) method used to estimate the model parameters. Inversion results obtained for simulated data in ideal and non-ideal (i.e., more realistic) cases are shown in Section 4. Finally, some conclusions are given in Section 5.

Chapter 2

Parameterization of the environment

The parameterization of the ocean environment is a delicate issue since the inversion results depend on the environment model adopted while the form of the real ocean waveguide is usually unknown. An inappropriate model can be a source of mismatch, a situation where the minimum misfit does not correspond to the true ocean properties, and can lead to poor estimates. Usually, independent *a priori* information guides the choice of the model. When modeling a range-dependent environment, the choice of the model also depends on the desired accuracy of the estimates. In our case, since we were first interested in detecting mesoscale ocean features rather than detailed mapping, a coarse model was used to represent the ocean.

In this model (see fig. 2.1), the water layer is gridded into three vertical cells (C_1, C_2 and C_3) of variable size. Each cell has an independent sound-speed profile and represents a water mass entity. More specifically, the middle cell represents the water mass with abnormal temperature that we want to estimate. Obviously, this representation would not be a pertinent choice to model an environment which properties vary smoothly and continuously with range. However to detect sharp fronts, such a model appears as a good first approximation. In addition, the use of vertical range limits for the middle cell is a simplification that is not unrealistic when modeling an upwelling since the water mouvement is mainly upwards. The rest of the model consists of a sediment layer laying over a semi-infinite substrate. Each layer (or cell) is characterized by its density, thickness, P- and S-wave velocities and attenuations.

For tomography purposes, the traditional approach to model the sound speed in the water is to use empirical orthogonal functions (EOFs). This method has been increasingly used since it can provide a high accuracy despite only a few coefficients/parameters are required. On the other hand, a major constraint in using EOFs is that one already needs a good knowledge (through direct measurements) of the ocean's properties to be able to calculate the eigenfunctions. In order to have eigenfunctions that accurately characterize both range and time variability of the sound speed, one needs a relatively large amount of measurements. However, the basic idea behind tomography, or any other remote-sensing method, is precisely to avoid direct measurements as much as possible. Therefore, we chose to estimate sound-speed points rather than EOF coeffcients.

In general, many points are necessary to get a good accuracy of the sound speed. On the other hand, estimating a large number of sound-speed points is an heavy task for an optimization method such as MFI. Once again, considering that our objective was primarily detection rather than accurate mapping of temperature anomalies, we chose a coarse representation of the sound speed that involved few but relevant parameters to

estimate. In this representation, the sound-speed profiles are defined with only three points: the sound speed in the homogenous sea-surface layer, at the lower limit of the thermocline and at the seafloor. Between the depth points, the inverse of the sound-speed squared varies linearly with depth.

The parameters to estimate are the three sound speeds of the middle-cell profile. (The sound speeds in the two other cells are suposed to be known.) In order to have a realistic and flexible model, the upper and lower limits of the thermocline ($d3$ and $d4$) are also estimated, as well as the range limits of the middle cell (R_1 and R_2).

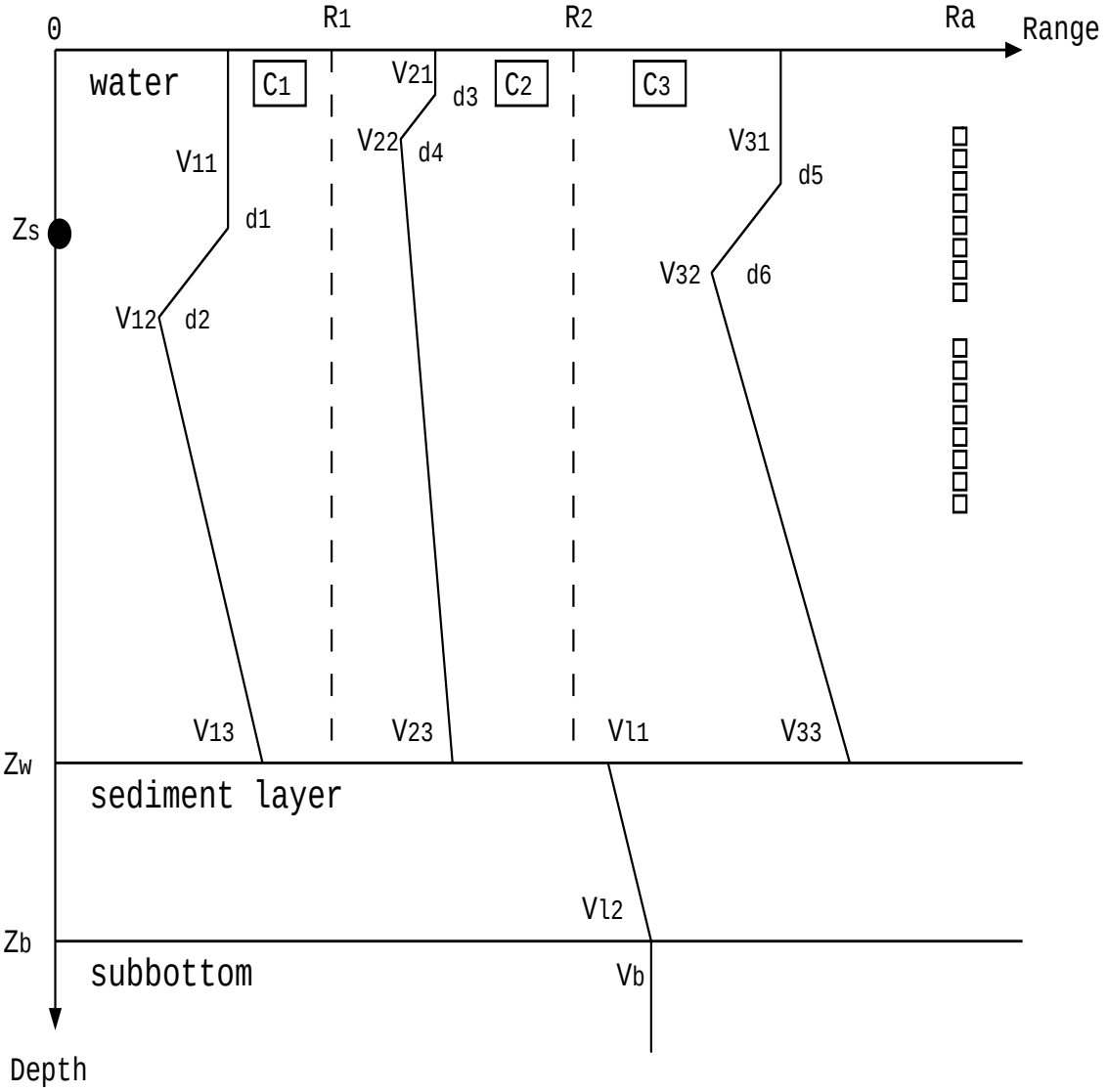

Figure 2.1: *Model of the ocean waveguide. The acoustic source is located at range 0, the vertical line of receivers at range R_a.*

Chapter 3

Matched-field inversion

In MFI, the estimation of model parameters consists in determining the optimum set of parameters that minimizes the misfit between the measured pressure field and the modeled field calculated for specific parameter values. This section briefly describes the different components of the MFI: the acoustic propagation code that calculates the modeled pressure fields, the cost function that quantifies the misfit, and the search algorithm that samples the parameter space in order to minimize the misfit.

3.1 Propagation code

In order to have a good compromise between accuracy and computational time, all pressure fields (simulated data and replica) were calculated using the SACLANTCEN coupled-mode code C-SNAP [4]. C-SNAP divides a range-dependent environment into several range-independent sections and can therefore handle waveguide models such as the one shown in fig. 2.1.

3.2 Objective function

To quantify the misfit between the data and replica fields, the frequency-incoherent Bartlett processor was used. The processor can be described as follows. Let $\hat{\mathbf{D}}(\mathbf{f})$ represent the normalized data pressure field measured at frequency f, and $\hat{\mathbf{P}}^*(\mathbf{m}, f)$ represent the normalized replica field calculated for the model of parameters $\mathbf{m}$. When the fields have N_f frequency components, the cost function to minimize is given by:

$$E(\mathbf{m}) = 1 - \frac{1}{N_f} \sum_{k=1}^{N_f} |\hat{\mathbf{P}}^*(\mathbf{m}, f_k)\hat{\mathbf{D}}(f_k)|^2. \tag{3.1}$$

3.3 Search algorithm

Due to the size of the parameter space and the non-linearity of the problem, neither an exhaustive nor a local search (gradient-type search) were a suitable approach to sample the parameter space. Instead an hybrid algorithm, the simplex genetic algorithm (SGA), was used. This algorithm combines the downhill simplex (DHS) [5] and genetic algorithm (GA) [6] for the local and global search respectively; and has shown good performances in previous inversions [7].

Chapter 4

Simulated study

In order to test the inversion method, it was first applied to synthetic data in the ideal case where there was no source of mismatch. It was then applied to more realistic cases when noise was added to the data and when the waveguide models used to calculate the data and replica were different.

4.1 Ideal case

4.1.1 Synthetic data

The baseline environmental model used to generate synthetic data sets is illustrated in fig. 2.1. The vertical array was made of two sections of eight receivers. Since the computational time increases linearly with the number of frequencies, the pressure fields were calculated only at 250 and 500 Hz. The value of the time and range-independent parameters of the waveguide are given in tab. 4.1. Synthetic time and range-dependent sound-speed profiles were derived from temperatures and salinities measured in an area featuring a cold filament [8] (see fig.4.1). A total of 11 time windows were selected to represent the apparition and evolution of a cold filament. In the first time window, the sound-speed profiles were identical in all three cells (range-independent ocean). The profiles of the middle cell are illustrated in fig. 4.2. The profiles in the two other cells did not vary with time and were known during the inversion. (In practice, profiles in cells C_1 and C_3 can be estimated by measuring the salinity and temperature profiles at the source and array locations.) The width of the middle cell randomly varied in time within the [11.95 - 12.05 km] interval while the horizontal distance between the source and the middle-cell front (R_1) varied between 10.95 and 11.05 km. With such a geometry, the middle cell was centered between the source and the array, and its width slightly larger than C_1 or C_3.

4.1.2 Inversions

The inversion method was applied three times to the data of each time window. Approximately 10000 sets of parameters were tested in each inversion with an initial population of 35 random sets. All known parameters of the waveguide were set to their true value (see tab. 4.1) such that, in theory, a global minimum misfit of zero could be reached

Table 4.1: *Time and range-independent parameters*

Parameter	**True value**
Geometric	
Range of the array R_a (km)	33.5
Shallowest receiver of section 1 (m)	50
Shallowest receiver of section 2 (m)	146
Distance between receivers (m)	4
Source depth Z_s (m)	90
Water depth Z_w (m)	400
Sediment layer	
P-wave velocity at top V_{l1} (m/s)	1600
P-wave velocity at bottom V_{l2} (m/s)	1620
Density ρ_l (g/cm^3)	1.4
S-wave velocity V_{ls} (m/s)	0
P-wave attenuation α_{ls} (dB/λ)	0.1
S-wave attenuation β_{ls} (dB/λ)	0
Lower interface depth Z_b (m)	420
Subbottom	
P-wave velocity V_b (m/s)	1800
Density ρ_s (g/cm^3)	2
S-wave velocity V_{bs} (m/s)	0
P-wave attenuation α_{bs} (dB/λ)	0.5
S-wave attenuation β_{bs} (dB/λ)	0

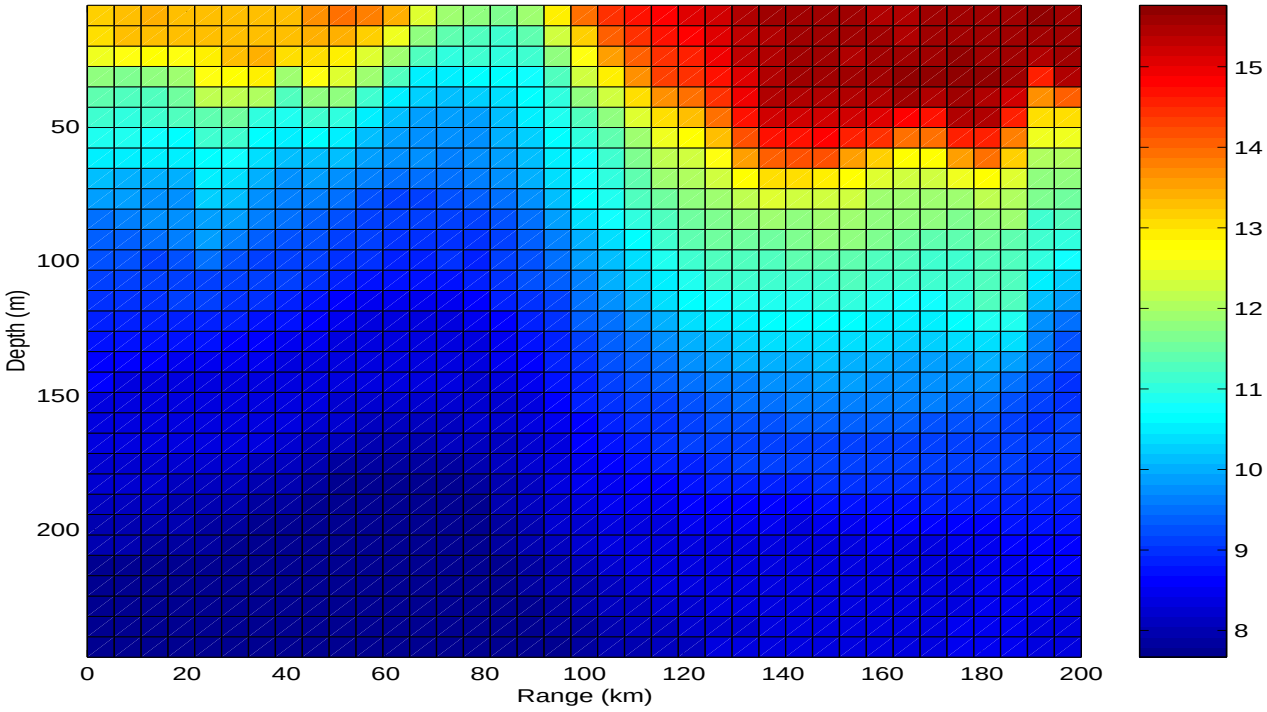

Figure 4.1: *Spatial variations of the temperature in a region featuring an upwelling filament .*

during the inversion. The search intervals were identical in all inversions and are given in tab. 4.2. In practice, the sound speed in the surface layer and at the bottom were defined by positive perturbations of the sound speed at the lower part of the thermocline:

$$V_{21} = V_{22} + \upsilon_1; V_{23} = V_{22} + \upsilon_2; \tag{4.1}$$

and υ_1 and υ_2 were the parameters to estimate rather than V_{21} and V_{23}. The purpose of this change of variables was to reduce the number of possible solutions by introducing meaningful constraints. In practice, the choice of the intervals for the range limits R_1 and R_2 would require *a priori* information such as satellite images of sea-surface temperature.

Table 4.2: *Search intervals for the unknown parameters*

Parameter	**Search interval**
Sound-speed in water (m/s)	1480-1510
Upper limit of the thermocline $d3(m)$	2-50
Lower limit of the thermocline $d4(m)$	65-210
Range limit R_1 (km)	9-11
Range limit R_2 (km)	21-23

The set of parameters corresponding to the minimum misfit encountered during the three inversions carried out for each time window was considered as the parameter estimates. Estimates of the sound-speed profiles and of the range limits of the middle cell are given in figs. 4.3 and 4.4 respectively. The cold-water raising is clearly visible and the range limits are well estimated. Since the environment is range independent in the first time window, the range limits are meaningless for this particular window, and so are their estimates (outfitters in fig. 4.4). A more physical representation of the inversion results is given in fig. 4.5 which shows the difference between the corresponding true and estimated sea-temperature profiles. The maximum and average absolute error (over depth and time) are less than 0.16 and $0.02°C$ respectively. (The absolute temperatures in the profiles range between 7.5 and $13°C$.) These results show that, for this particular configuration, it is possible to not only detect the cold water upwelling but also to obtain an accurate mapping of the sound-speed/temperature profile. However, regarding the temperature estimate, one has to take into account that the temperature profiles were deduced from the estimated sound-speed profiles and the exact salinity profiles. In practice, an error of 1 % in salinity (i.e., approximately the difference introduced by the filament) would lead to a temperature error of $0.4°C$. Therefore temperature estimates must be handled carefully. It is worth noting that the misfits corresponding to these estimates were small (between 10^{-6} and 10^{-4}) but were not the global minimum, i.e., the machine accuracy 10^{-16}. Considering that 1) the parameter accuracy was already relatively good for misfits between 10^{-6} and 10^{-4}, 2) misfits smaller than 10^{-4} were unexpected in realistic scenarios, and 3) we were mainly interested in global detection rather than accuracy, we kept the number of iterations equal to 10000 in the rest of the study. Each inversion was then 45 minutes long approximately.

4.1.3 Effect of middle-cell size and location on the inversion results

The sensitivity of the pressure field to the sound-speed/temperature anomaly, and therefore the performance of the inversion method, vary with the properties of the anomaly:

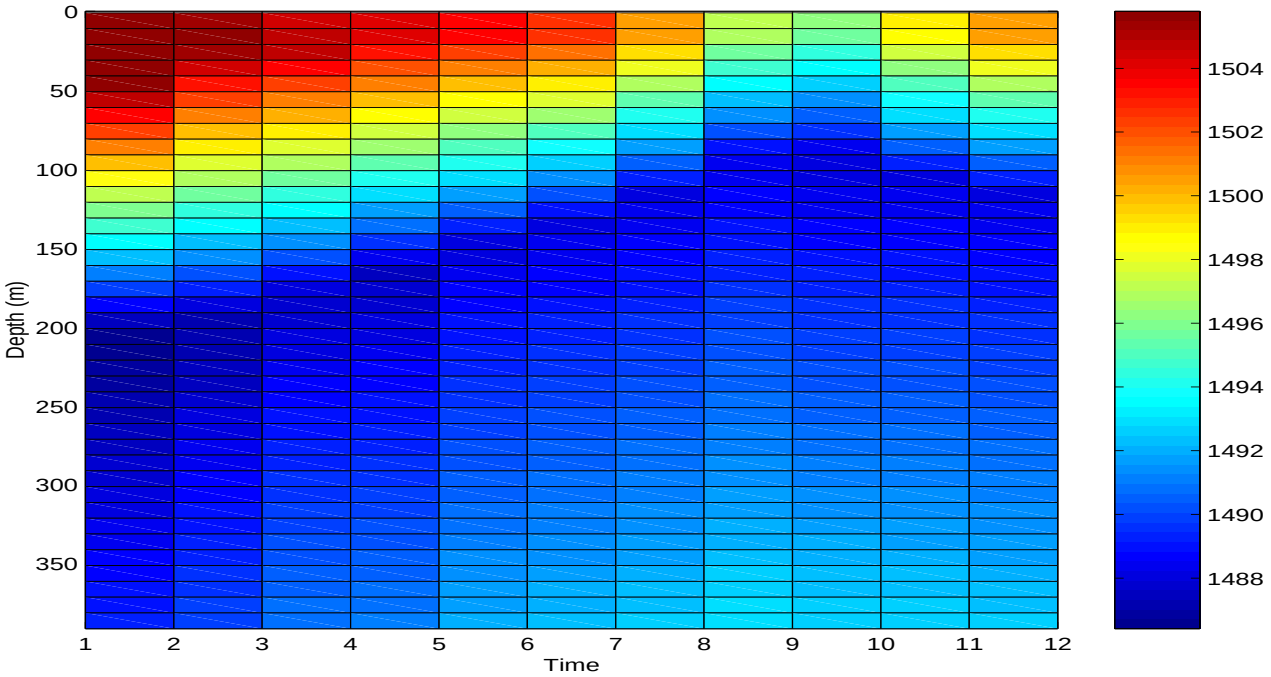

Figure 4.2: *Time variations of the sound-speed profiles in the middle cell. These profiles define the true environment.*

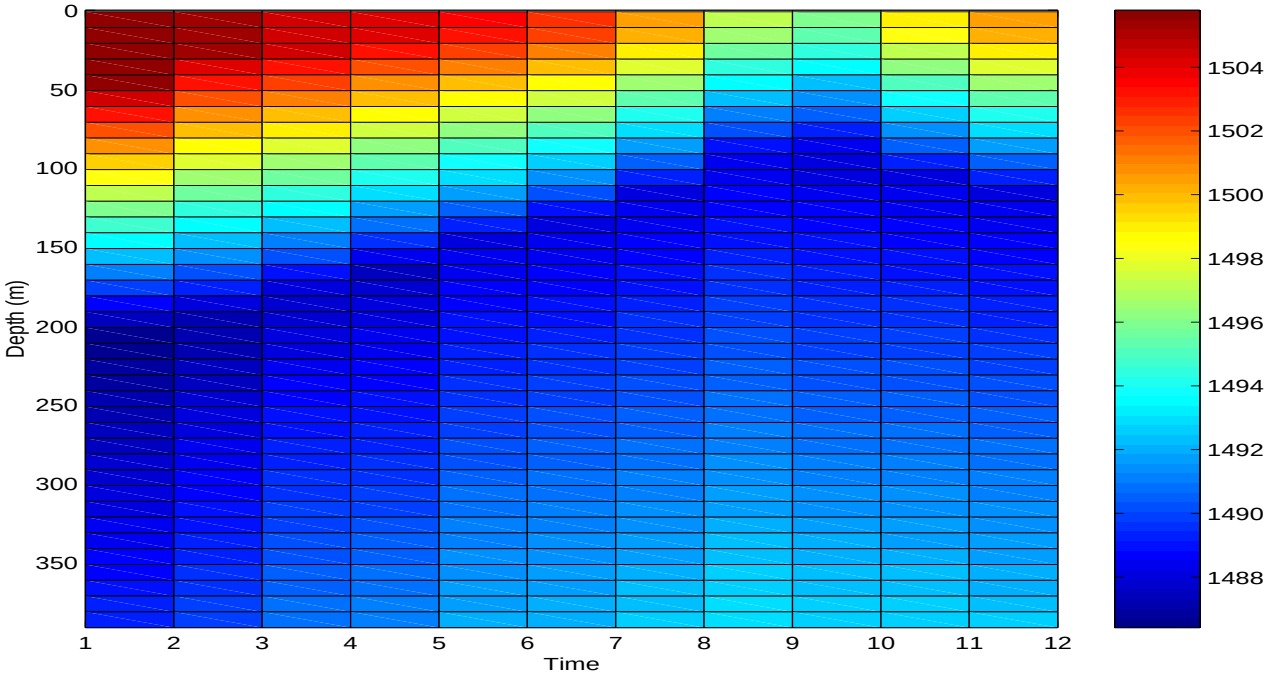

Figure 4.3: *Estimated sound-speed profiles in the middle cell.*

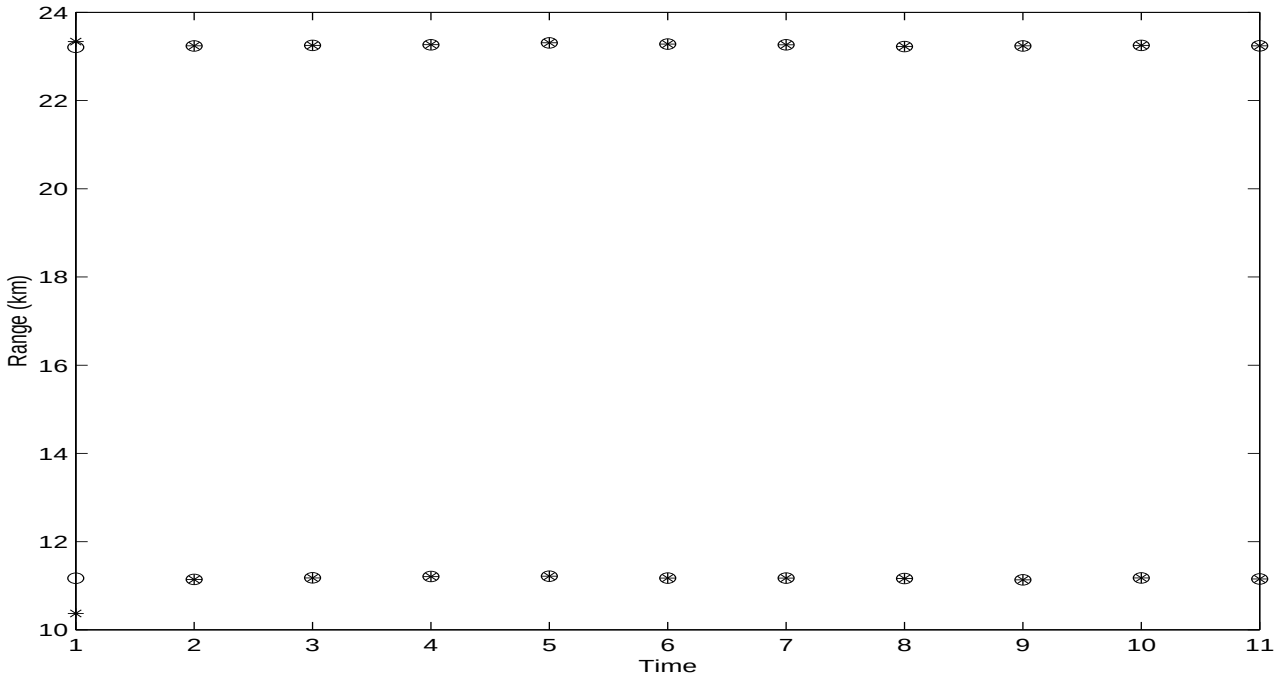

Figure 4.4: *True (circle) and estimated (star) range limits of the middle cell.*

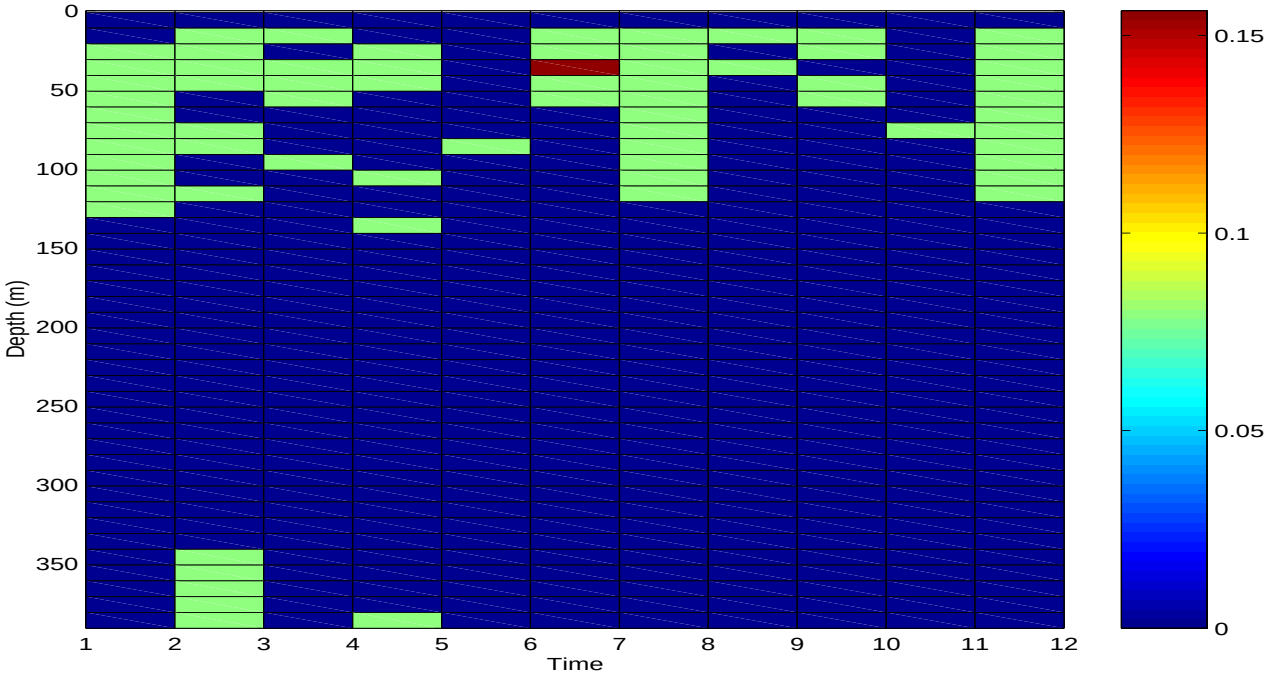

Figure 4.5: *Absolute error between the true and estimated temperature profiles in the middle cell.*

dimension, location and sound-speed itself. To illustrate the effect of these properties, series of inversions were repeated for three sizes of the middle cell (12, 7 and 2 km) and three locations (R_1=5, 11 and 17 km from the source). From one inversion to another, all other parameters were identical, including the inversion parameters (number of iterations, size of GA population etc...). For each inversion, the parameter mean relative error ε was calculated according to Eq. 4.2:

$$\varepsilon = \frac{1}{N_p} \sum_{p=1}^{N_p} \frac{|m(p) - m_t(p)|}{m_t(p)}, \tag{4.2}$$

where N_p is the number of parameters (N_p =7 here), $m(p)$ is the estimate of the p^{th} parameter and $m_t(p)$ is its true value. The variations of the error with time for all cases are given in fig. 4.6. The general observation is that the parameter estimates degrade for the time windows 8, 9 and 10 which correspond to the cases where the homogenous sea-surface layer is very thin (<8 m). Then, the results show that for identical inversion conditions the best performance of the inversion method is obtained when the middle cell is centered between the source and the array. This region is most likely to have the best sampling in terms of acoustic energy. The effect of the cell width is less clear as the 12 km and 2 km cases gave similar variations. However, in any case, it is possible to obtain a very good approximation of the filament evolution (see figs. 4.7 and 4.8).

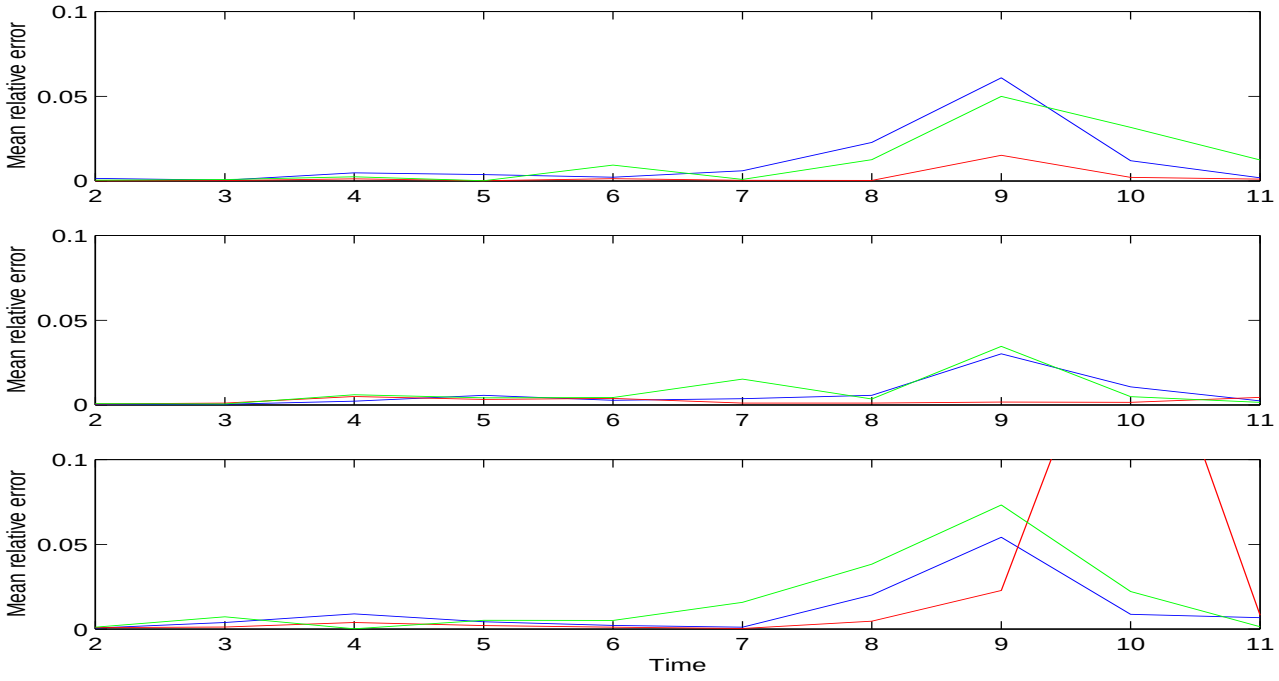

Figure 4.6: *Variations of the parameter mean relative error (ε) with the middle cell location (top: R_1=5 km, middle: R_1=11 km, bottom: R_1=17 km) and width (blue: 12 km, red: 7 km, green: 2 km).*

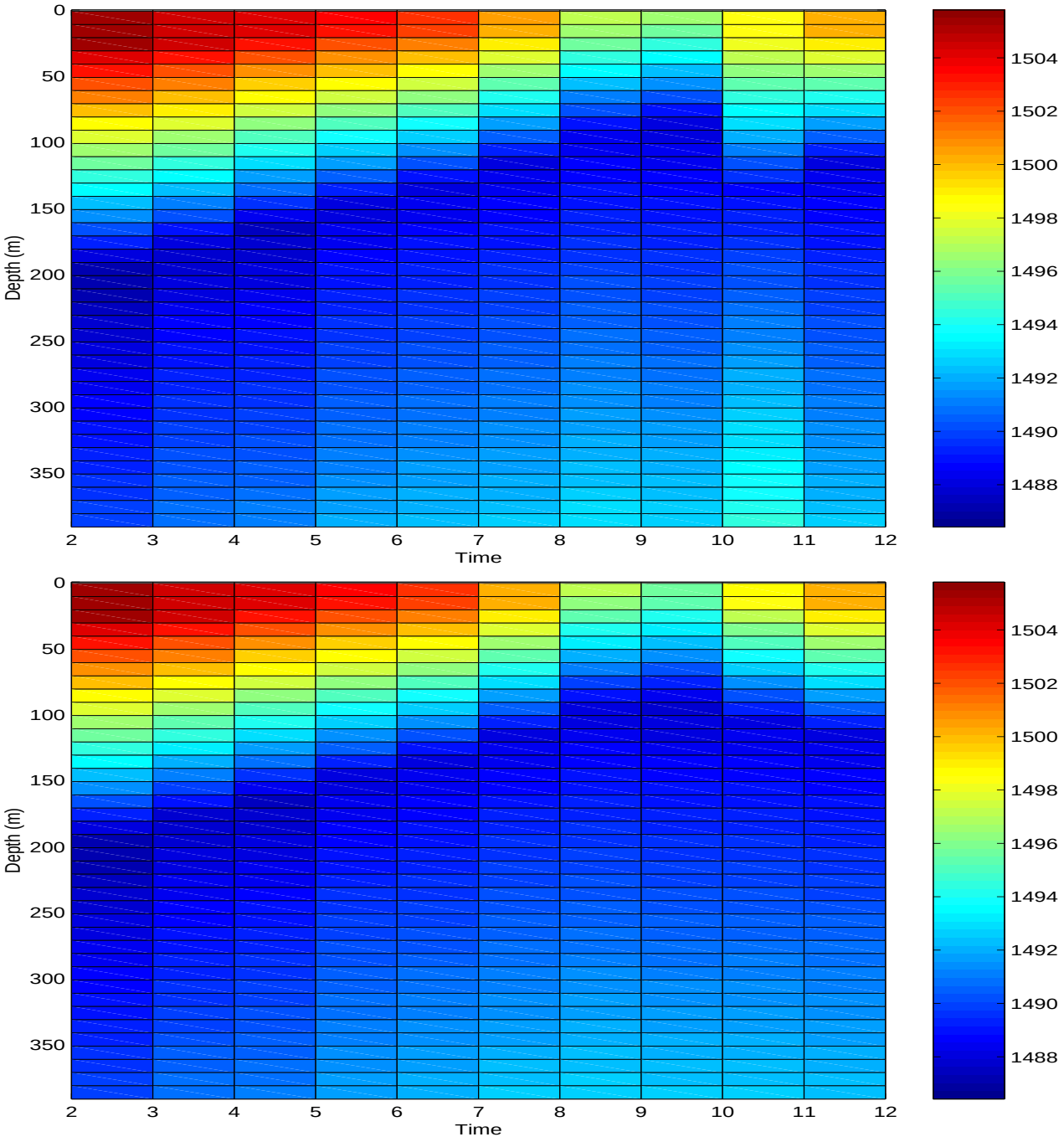

Figure 4.7: *Estimated sound-speed profiles in the middle cell located 17 km from the source and with a width of 7 km (top) and 2 km (bottom). The true profiles are given in fig. 4.2.*

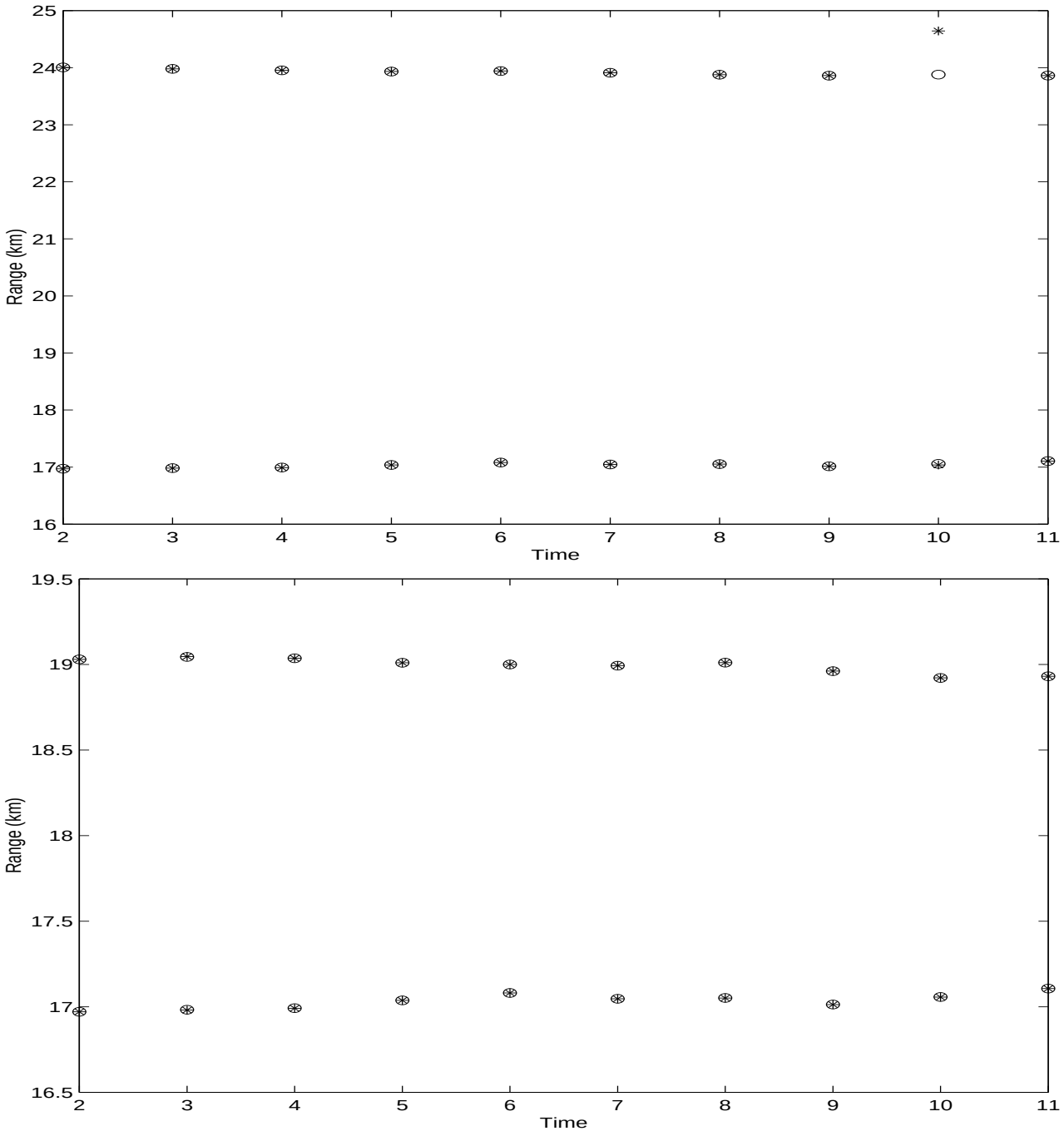

Figure 4.8: *True (circle) and estimated (star) range limits of the middle cell located 17 km from the source.*

4.2 Non-ideal cases

In reality, ideal cases such as the one treated above do not occur. Therefore, it is important to know the limitations of the inversion method for more realistic conditions. Here we investigate two potential sources of mismatch: the presence of noise in the data and an erroneous parameterization of the waveguide. These situations imply a non-null global minimum misfit and the fact that this global minimum may not correspond to the true parameters. Since MFI works as a "black box" where the inversion is only driven by minimizing the misfit function, a case-by-case study is necessary to know the effect of a particular mismatch on the parameter estimates.

4.2.1 Effect of correlated noise on the inversion results

Correlated noise $\mathbf{N}(f)$ was added to the original synthetic pressure field $\mathbf{P}(\mathbf{m}, f)$ to generate a new data set $\mathbf{P}'(\mathbf{m}, f)$ according to:

$$\mathbf{P}'(\mathbf{m}, f) = \mathbf{P}(\mathbf{m}, f) + K \cdot \mathbf{N}(f), \tag{4.3}$$

where K is a vector of real numbers that allows to set the level of noise at each hydrophone h to a given value (see Eq. 4.6). The noise itself was a sum of two components:

$$N_h(f) = \alpha(f) + \beta_h(f), \tag{4.4}$$

where $\alpha(f)$ and $\beta_h(f)$ were complex, zero-mean, Gaussian-distributed random numbers. The fact that for a given frequency, the pressure fields at all hydrophones contained an identical component (α) increased the degree of correlation between the pressure fields. On the other hand, β simulated the white-noise component (ambient noise) of the measured pressure fields. Let σ_α and σ_β be the standard deviations of α and β. The noise correlation between hydrophones h and j is given by:

$$\begin{aligned} C_{hj}(f) &= E[N_h(f)N_j^*(f)] \\ &= E[(\alpha(f) + \beta_h(f))(\alpha(f) + \beta_j(f))^*] \\ &= E[(\alpha(f)\alpha^*(f))] + E[\beta_h(f)\beta_j^*(f)] \\ &\quad + E[\beta_h(f)\alpha^*(f)] + E[\alpha(f)\beta_j^*(f)] \end{aligned} \tag{4.5}$$

Since α and β are independent noise realizations, the last two terms are nul and the correlation is reduced to $C_{hj}(f) = \sigma_\alpha$ for $j \neq h$, and $C_{hh}(f) = \sigma_\alpha + \sigma_\beta$ for $j = h$. In practice, σ_α and σ_β were set equal.

The performance of the inversion method was tested for two levels of noise: 10 and 5 dB, the signal-to-noise ratio (SNR) at the h^{th} hydrophone being defined by:

$$\mathrm{SNR}_h = 10 \times \log_{10} \left(\frac{\sum_{i=1}^{N_f} |P'_h(\mathbf{m}, f_i)|^2}{\sum_{i=1}^{N_f} |N_h(f_i)|^2} \right). \tag{4.6}$$

Inversions were carried out for a middle cell located 11 km from the source and with a width of 12 km. Except for the presence of the noise, the conditions of inversion were the same than for the ideal case. For a given SNR and time window, five different noisy data

sets were inverted. Estimates of the sound-speed profiles and range limits obtained with the smallest misfit out of these five inversions are shown in figs. 4.9 and 4.10 respectively. For comparison, the differences between estimated and true sea-temperature profiles are shown in fig. 4.11. The larger the noise, the larger the differences. The mean absolute error over depth and time is 0.056 and $0.126°C$ for 10 and 5 dB respectively. However, despite the presence of noise, the parameter estimates are relatively good and the evolution of the cold filament can still be well observed.

Since the global minimum is unknown, it is not possible to know if the inversion algorithm has reached it or not. One can only verify that the minimum misfit encountered is smaller than the misfit calculated for some particular parameter sets. Here, one obvious set to check is the set of true parameters, i.e., the parameters used to generate the noise-free pressure fields. As shown in fig. 4.12, the misfit calculated with the true parameters is not null and is larger than the minimum misfit encountered for each time window. Standing by itself, this result only stresses the ability of the inversion algorithm to reach regions of low misfit. However the sensitivity curves obtained for the ideal and $5dB$ cases (see fig. 4.13) provide additional insight in the problem as the two series of curves have very similar behavior and exhibit their global minimum at the parameter true values. Although the generalization to the entire parameter space (multi-dimensional space) is not feasible here, this result can explain the relative robustness of the parameter estimates to the presence of noise in the data.

4.2.2 Effect of model mismatch on the inversion results

In the above, the waveguide models used to calculate the simulated data and replica fields had the same geometry (three layers, three cells, flat bottom etc...). Here we are interested in increasing the complexity of the water layer in the true waveguide, while keeping the original parameterization of the replica waveguide in order to test the inversion method in a more realistic scenario. Among the possible approaches to make the waveguide more complex, we chose to introduce transition cells on each side of the middle cell. The parameters of these cells were set to average values between the middle cell and C_1 or C_3's parameters. The width of the transition cells varied between 250 and 750 m. The transition cells were overlapping the middle cell in the sense that C_1 and C_3 always had a constant width of 10 and 13 km respectively. The search intervals for the range limits were increased to 3 km wide to include the transition cells. Estimated profiles are given in figs. 4.14 to 4.16. The wider the transition cells, the larger the error in the middle-cell profile estimate. Here again, the error is larger for the time windows 8, 9 and 10. However, up to 500 m wide, the global picture of the cold water upwelling is well visible.
As for the noise case, the global minimum is unknown in all scenarios. However here, it is not possible to use the true parameters to verify the algorithm convergence to a low misfit region since the replica waveguide is defined by less parameters than the true waveguide. Nevertheless, for comparison purpose, a reference misfit was calculated with the true parameters of the middle cell. As shown in fig. 4.17, this reference is relatively large and always larger that the minimum misfit encountered during the series of inversions, indicating a good performance of the algorithm to reach regions of low misfit.

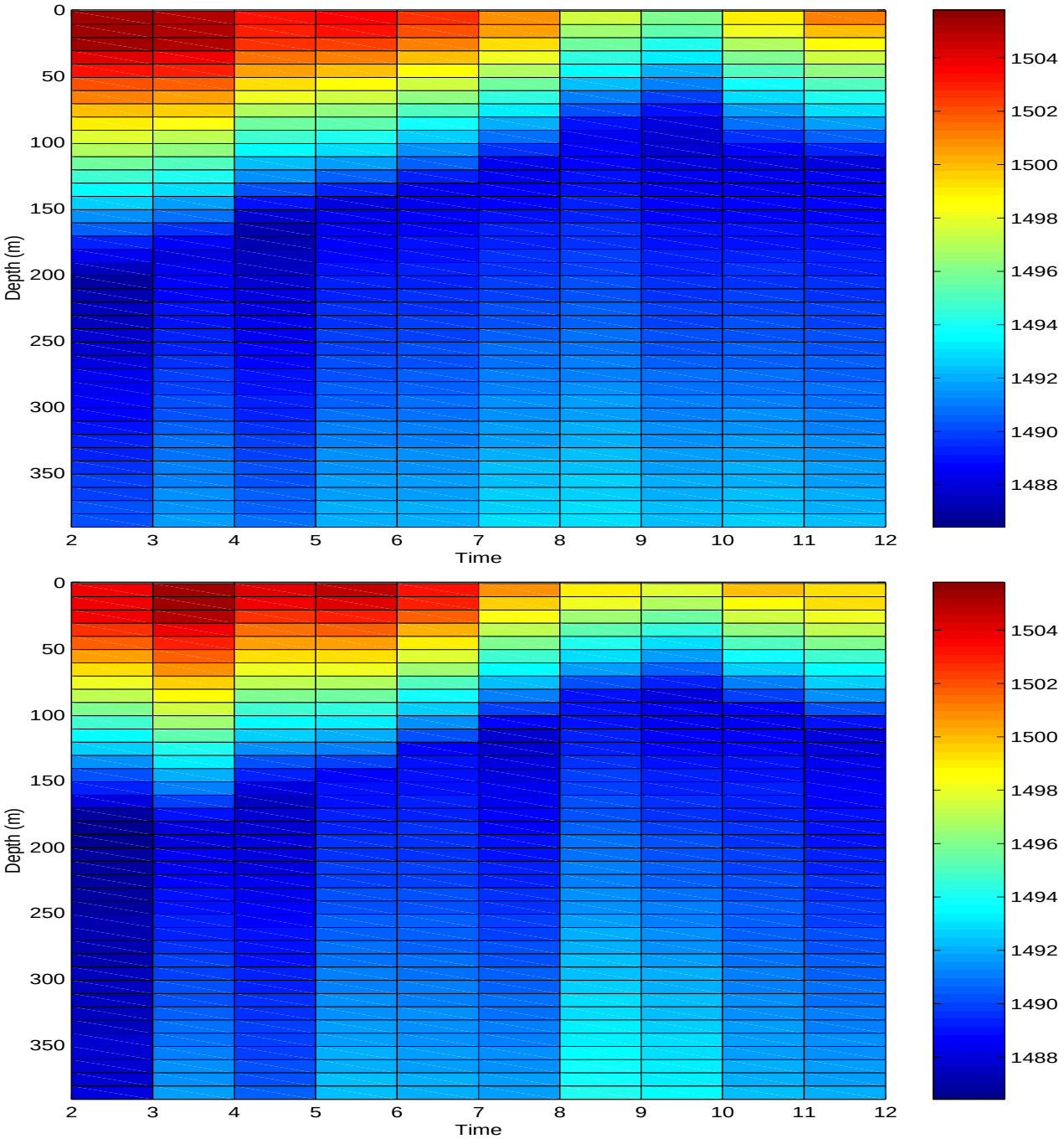

Figure 4.9: *Estimated sound-speed profiles in the middle cell for SNR=10 (top) and 5 dB (bottom). The true profiles are given in fig. 4.2.*

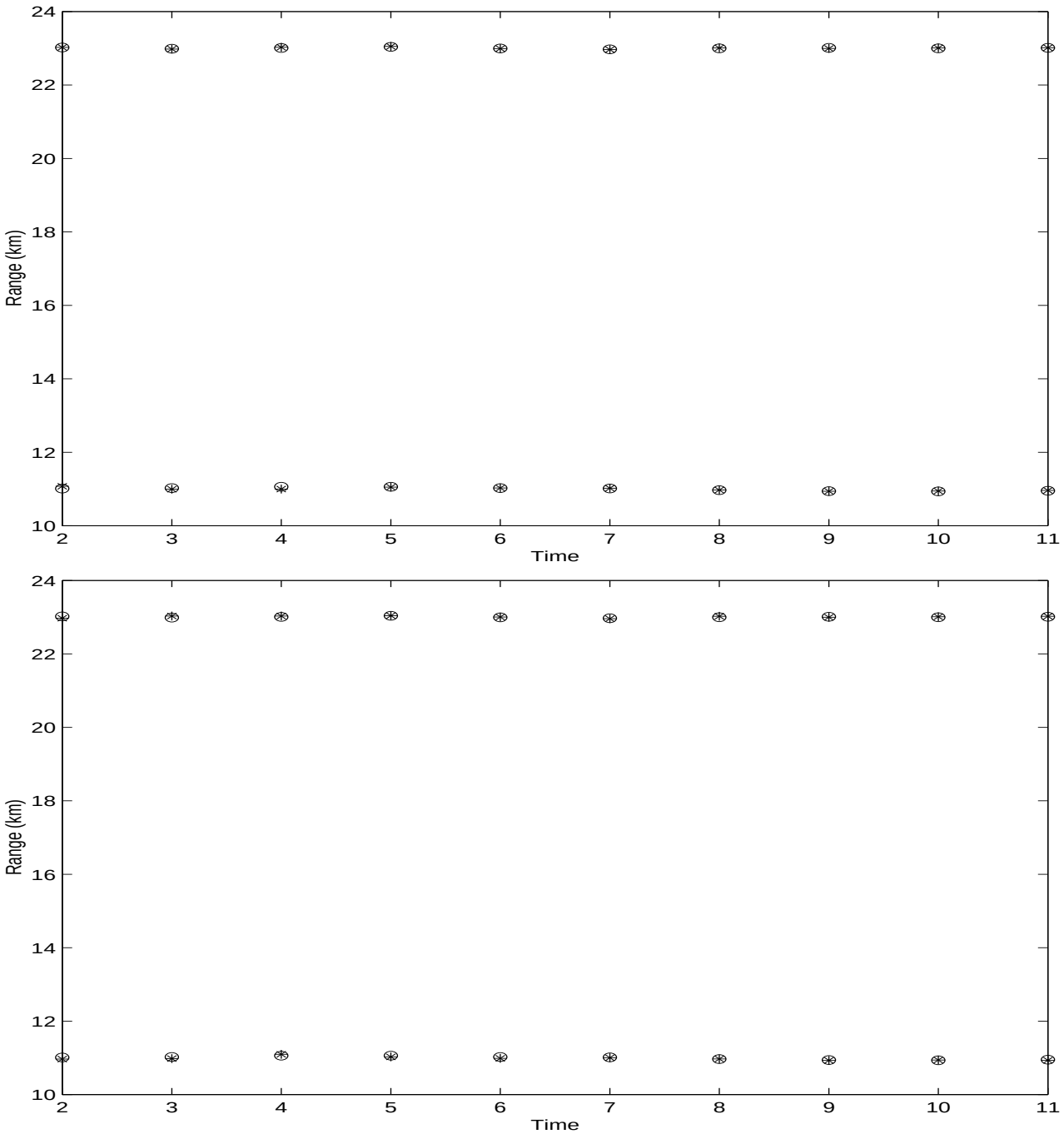

Figure 4.10: *True (circle) and estimated (star) range limits of the middle cell for SNR=10 (top) and 5 dB (bottom).*

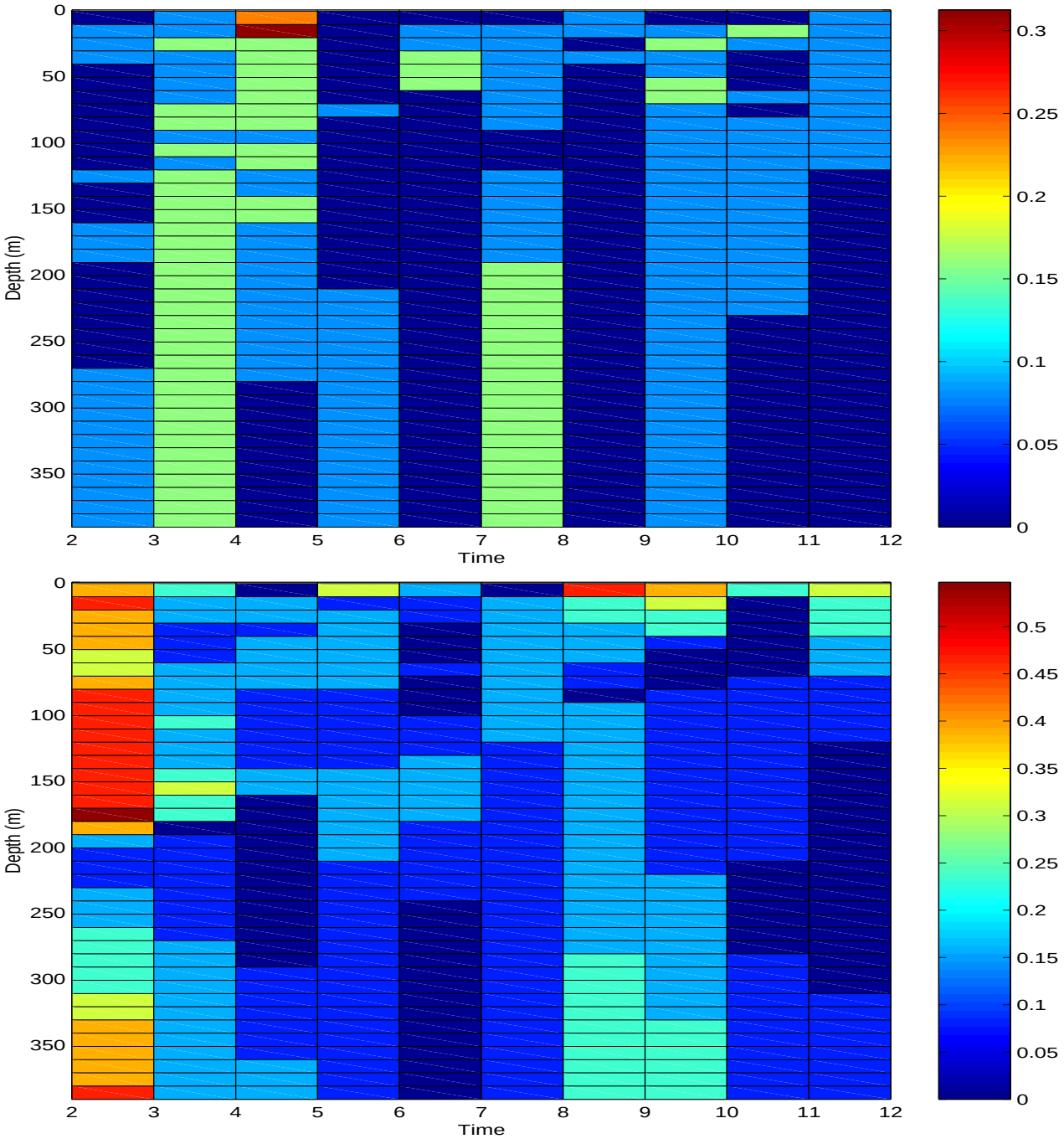

Figure 4.11: *Absolute error between true and estimated temperature profiles for SNR=10 (top) and 5 dB (bottom).*

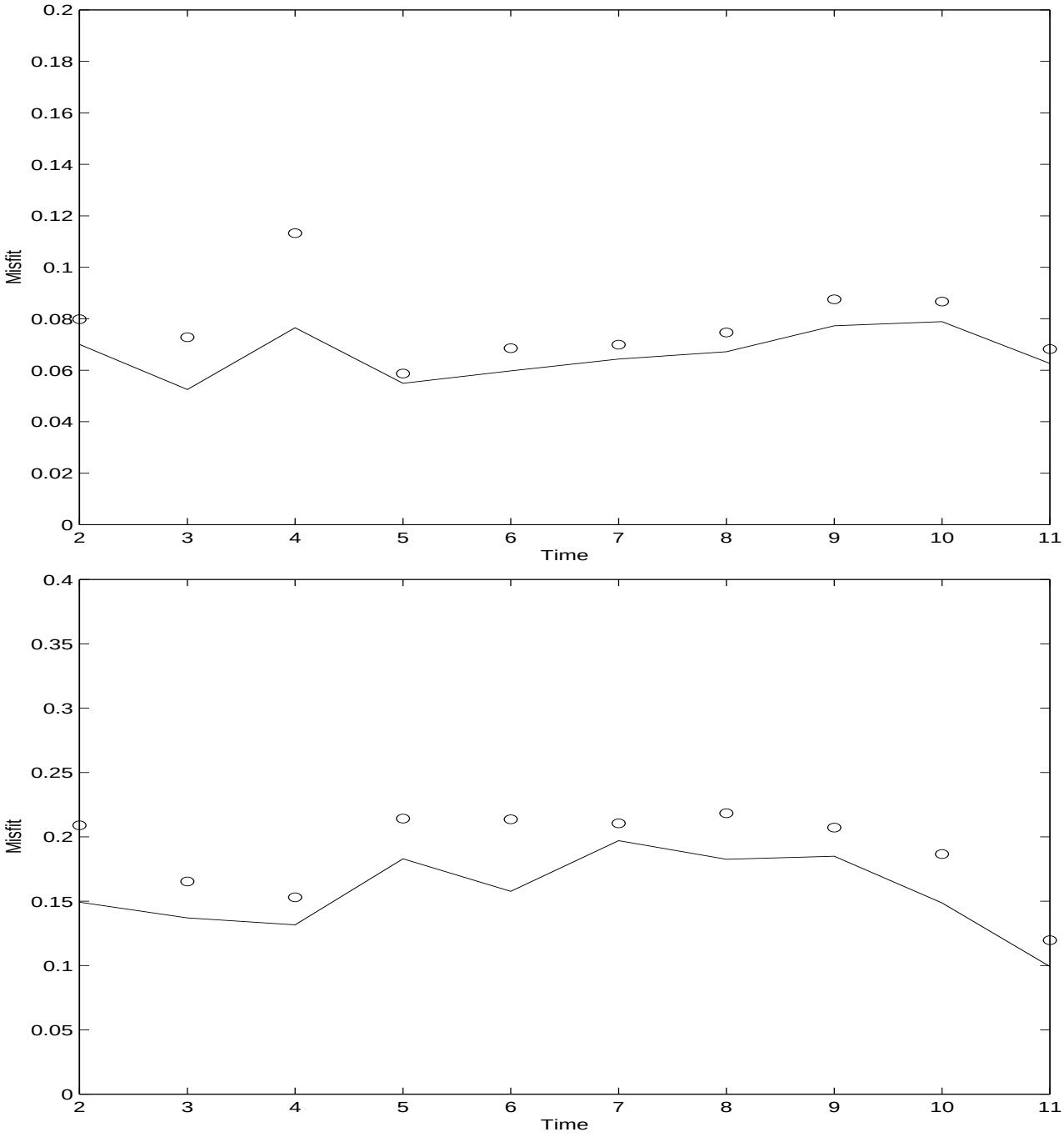

Figure 4.12: *Minimum misfit obtained during the inversions for SNR=10 (top) and 5 dB (bottom). The circles indicate the misfit calculated with the true parameters.*

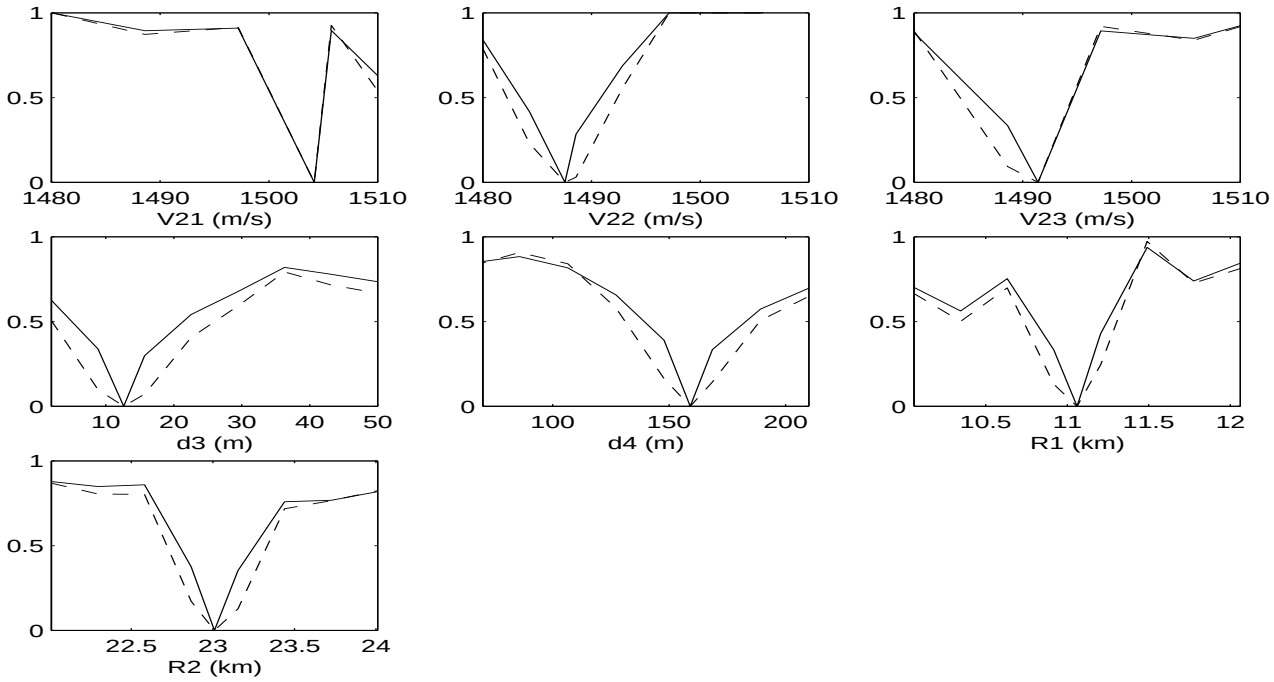

Figure 4.13: *Variations of the misfit with individual parameter, the remaining parameters being fixed to their true value for time window 4, cell width 12 km and distance from source 11 km. The dash line indicates the noise-free case. The solid line shows the average misfit obtained for 15 realizations of correlated noise with SNR=5dB.*

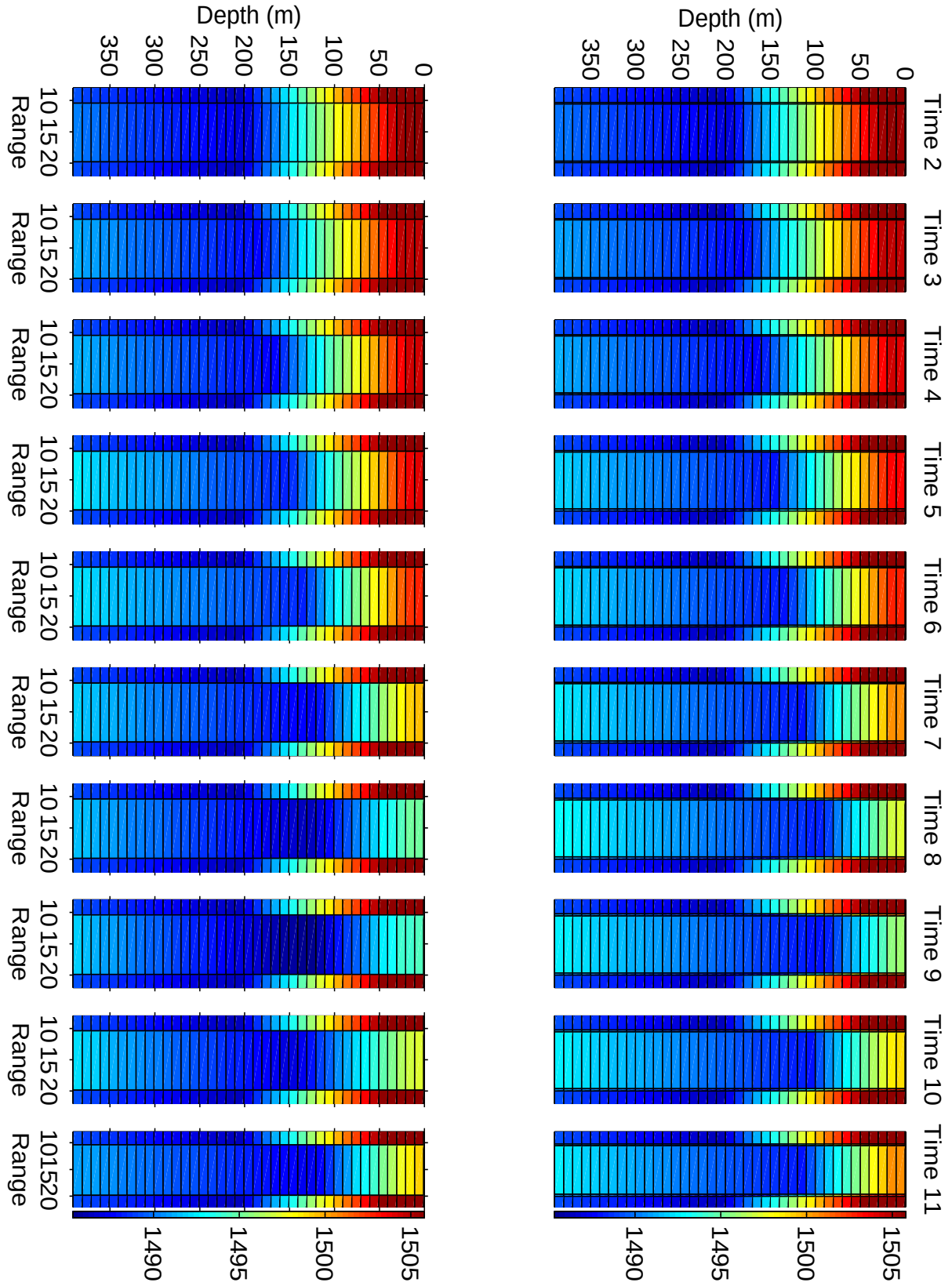

Figure 4.14: *Time variations of the true (top) and estimated (bottom) sound-speed profiles. Transitions cells are 250 m wide. Note that for clarity and emphasis on the middle cell properties, only part of cells 1 and 3 (C_1, C_3) is represented in each panel.*

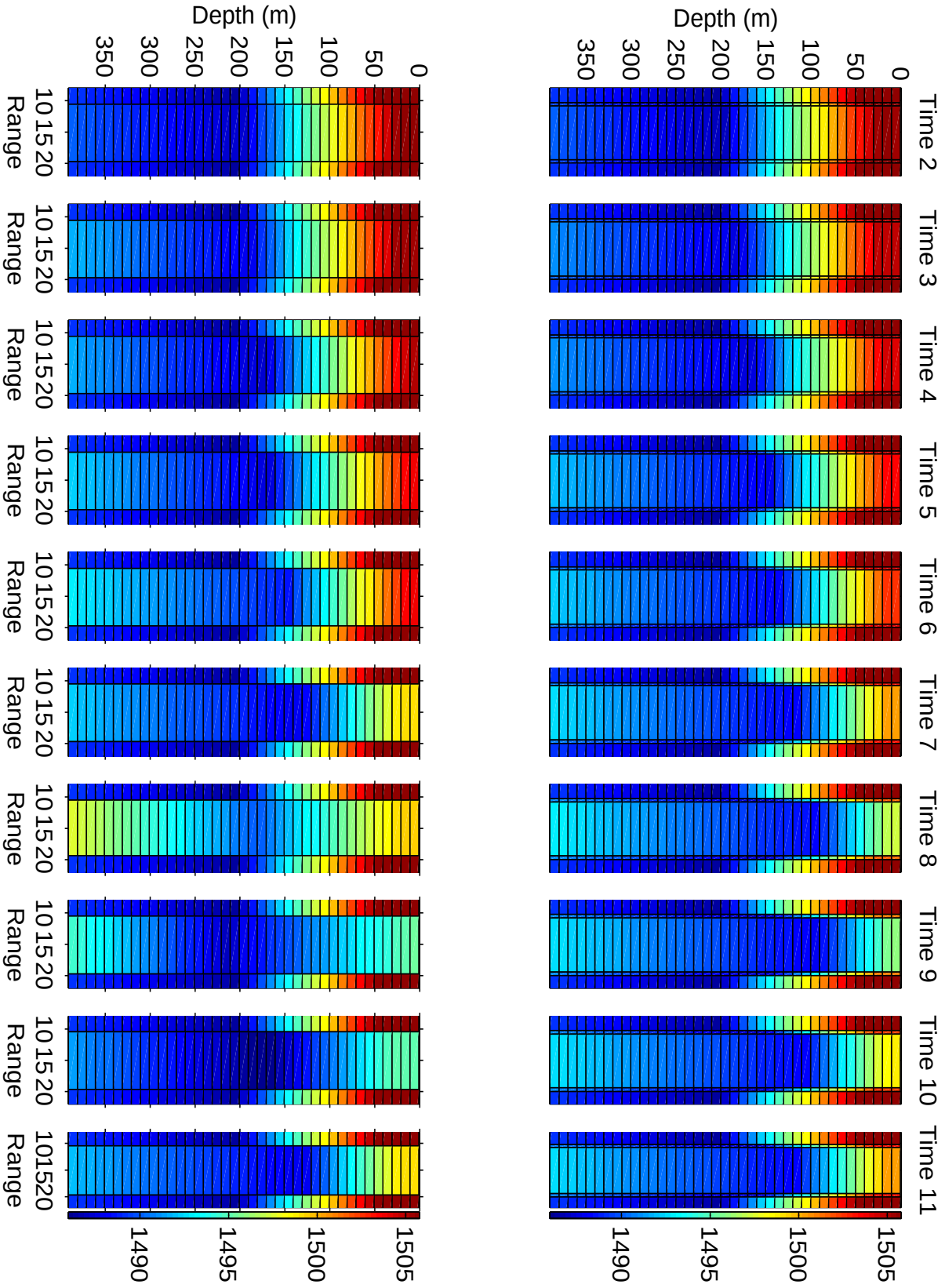

Figure 4.15: *Time variations of the true (top) and estimated (bottom) sound-speed profiles. Transitions cells are 500 m wide.*

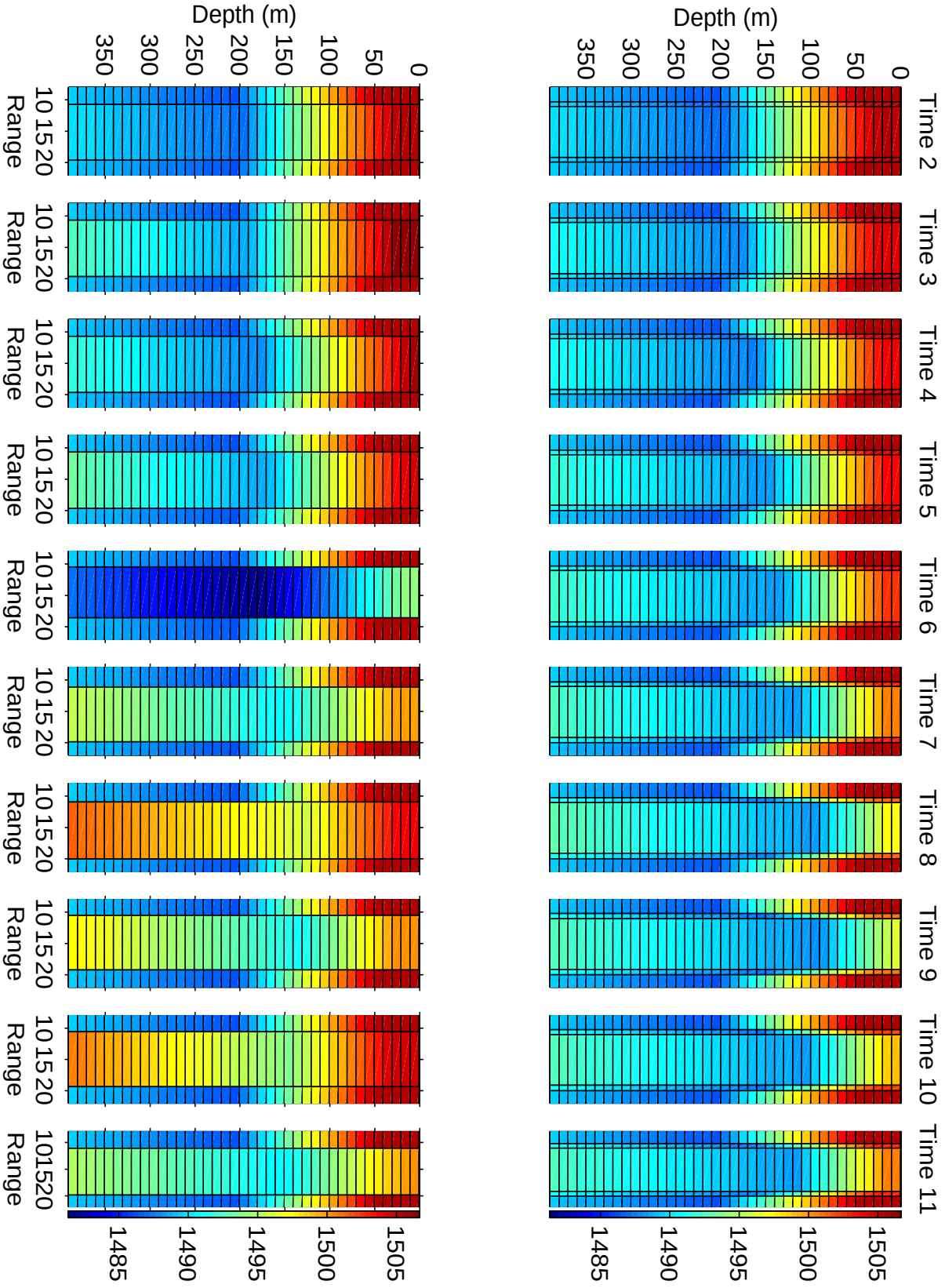

Figure 4.16: *Time variations of the true (top) and estimated (bottom) sound-speed profiles. Transitions cells are 750 m wide.*

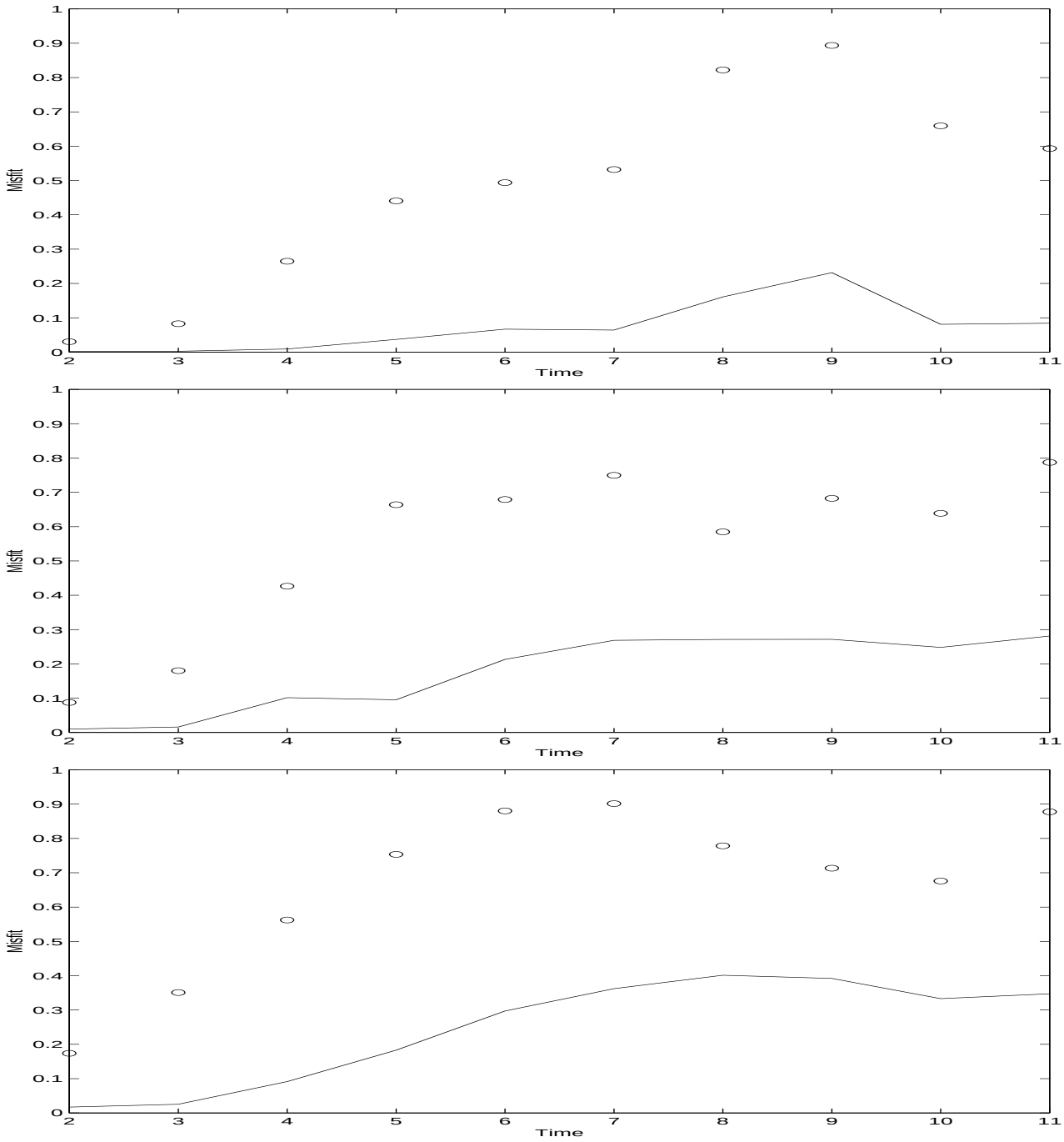

Figure 4.17: *Minimum misfit obtained during the inversions with model mismatch. The circles indicate the misfit calculated with the true parameters of the middle cell. From top to bottom, the width of the transition cells was 250, 500 and 750 m.*

4.3 Systematic study

As mentioned above, inversion results are case dependent and we obtained different accuracies on the parameter estimates depending on the location, width and sound-speed profile of the middle cell. In addition to these environmental parameters, the positions of the source and array also affect the inversion results. Those are interesting parameters to study since they are under human control and relatively easy to vary. In the following, the effect of the source-array distance (R_a), the depth of the hydrophones and the source depth (Z_s) are systematically investigated through different inversion scenarios (tab. 4.3). In all scenarios, the parameters not defined in tab. 4.3 were identical to those

Table 4.3: *Location of the source and hydrophones for the different inversion scenarios. The array is defined by the depth of the shallowest hydrophone in each of the two array sections.*

Scenario	$R_a(km)$	**Array** (m)	$Z_s(m)$
1	33.5	50, 146	90
2	27.5	50, 146	90
3	20.5	50, 146	90
4	33.5	114, 146	90
5	33.5	50, 82	90
6	33.5	50, 146	120
7	33.5	50, 146	70

given in tab. 4.1. No transition cells were present when calculating the simulated pressure fields but correlated noise was added to the data such that the SNR was 10 dB at each hydrophone. This level of noise corresponds to a realistic experimental situation. For each scenario, three inversions were repeated for 10 time windows (the range-independent profile was not investigated), three middle-cell widths (2, 7, 12 km), and three middle-cell locations (5, 11, 17 km). In each inversion, a different realization of correlated noise was used.

The parameter mean relative error corresponding to the minimum misfit encountered during the three inversions is shown in figs. 4.18 to 4.20 for the various scenarios. The absence of obvious trends with the array and source positions emphasizes the sensitivity of the pressure field to the various waveguide properties (the effect of different noise realizations is considered negligible here).
In the few cases where the error is larger than 5 (cases concentrated in time windows 7-10), the inversion algorithm consistently failed to find a minimum misfit smaller than the misfit calculated with the true value. This poor performance can be due to a greater complexity of the parameter spaces to sample (see example in fig. 4.21).
On average, the error is two orders of magnitude larger than the error found in the ideal case (fig. 4.6). However, in most cases, the upwelling is still clearly visible as shown in fig. 4.22 which illustrates the sound-speed estimates for a non-optimal result (red line of left bottom panel of fig. 4.19). For this particular case, the average temperature absolute error over time and depth is 0.14 $°C$.
Regarding the middle-cell properties, it is worth noting that, in most cases, the smallest errors are obtained when the cell is centered between the source and array.

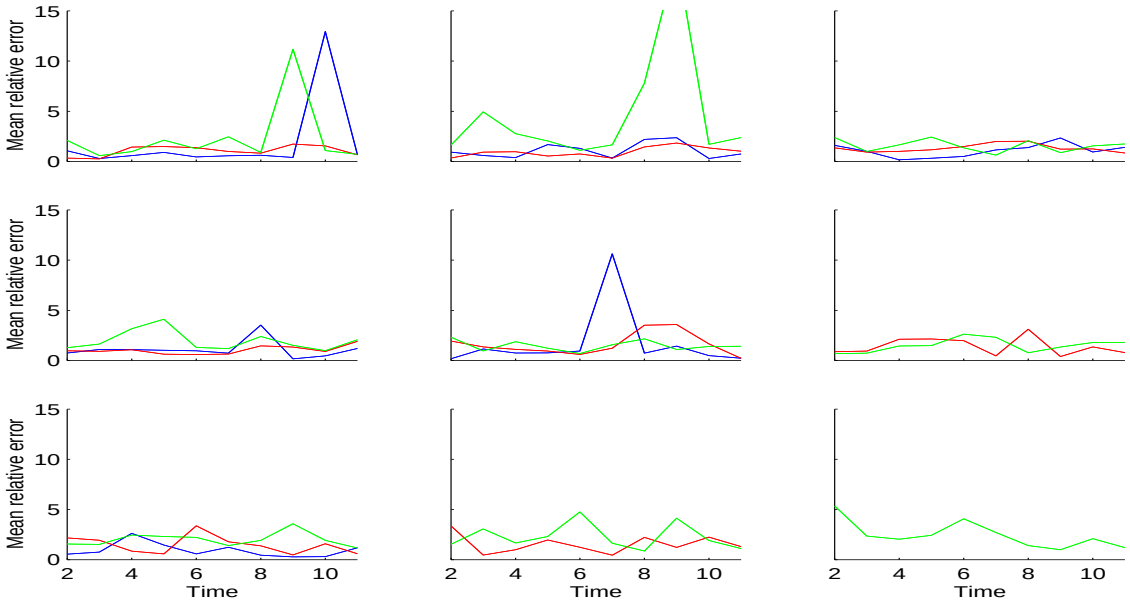

Figure 4.18: *Variability of the parameter mean relative error (ε) with the source-array distance, the position of the middle cell and the width of the middle cell. From left to right the source-array distance was 33.5, 27.5 and 20.5 km (scenarios 1-3). From top to bottom, the middle cell was 5, 11 and 17 km from the source. The colors indicate the width of the middle cell: blue for 12 km, red for 7 km and green for 2 km. The missing blue and/or red lines in some panels are cases where the R_2 range limit of the middle cell was beyond the array position. These cases were not investigated.*

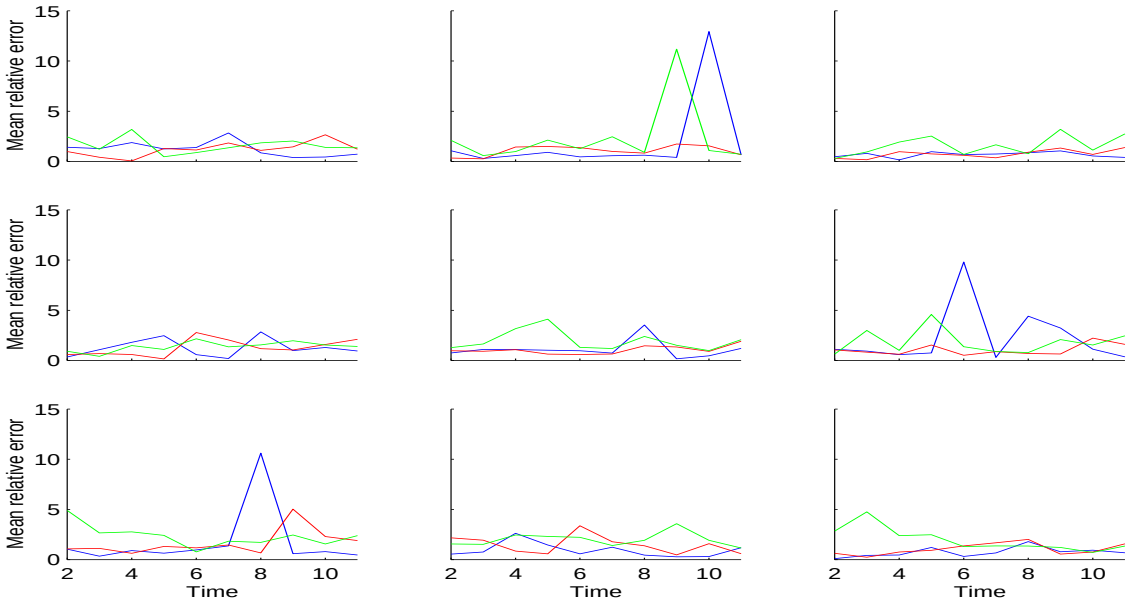

Figure 4.19: *Variability of the parameter mean relative error (ε) with the vertical position of the array, the position of the middle cell and the width of the middle cell. From left to right the depth of the shallowest receiver of the two array sections were $\{50, 82\}$, $\{50, 146\}$ and $\{114, 146\}$ m (scenarios 5, 1, 4). From top to bottom, the middle cell was 5, 11 and 17 km from the source. The colors indicate the width of the middle cell: blue for 12 km, red for 7 km and green for 2 km.*

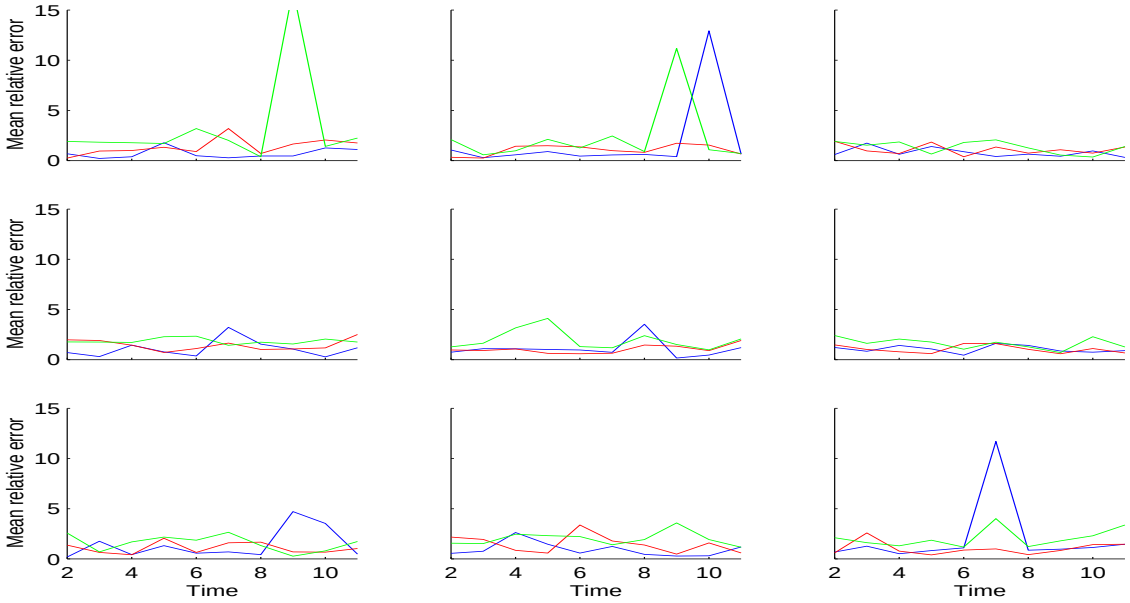

Figure 4.20: *Variability of the parameter mean relative error (ε) with the source depth, the position of the middle cell and the width of the middle cell. From left to right the source depth was 120, 90 and 70 m (scenarios 6, 1, 7). From top to bottom, the middle cell was 5, 11 and 17 km from the source. The colors indicate the width of the middle cell: blue for 12 km, red for 7 km and green for 2 km.*

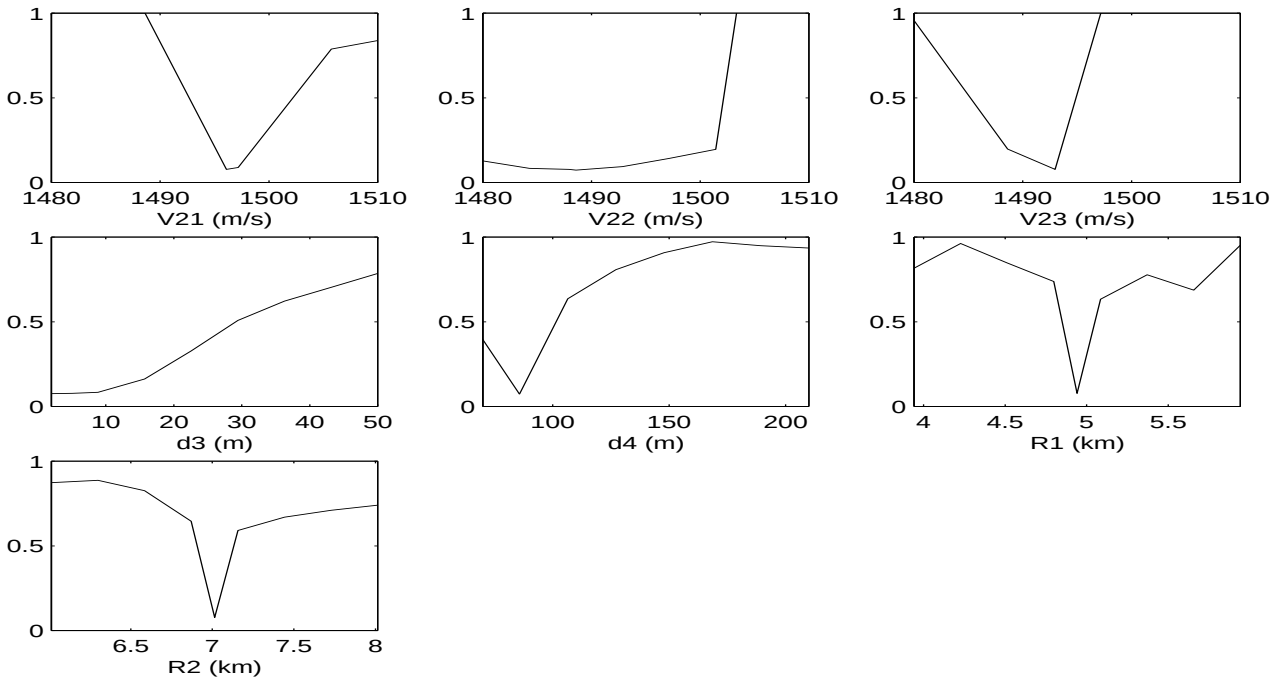

Figure 4.21: *Variations of the misfit with individual parameter, the remaining parameters being fixed to their true value for scenario 6, time window 9, cell width 2 km, cell position 5 km from source. The line shows the average misfit obtained for 10 realizations of correlated noise with SNR=10dB.*

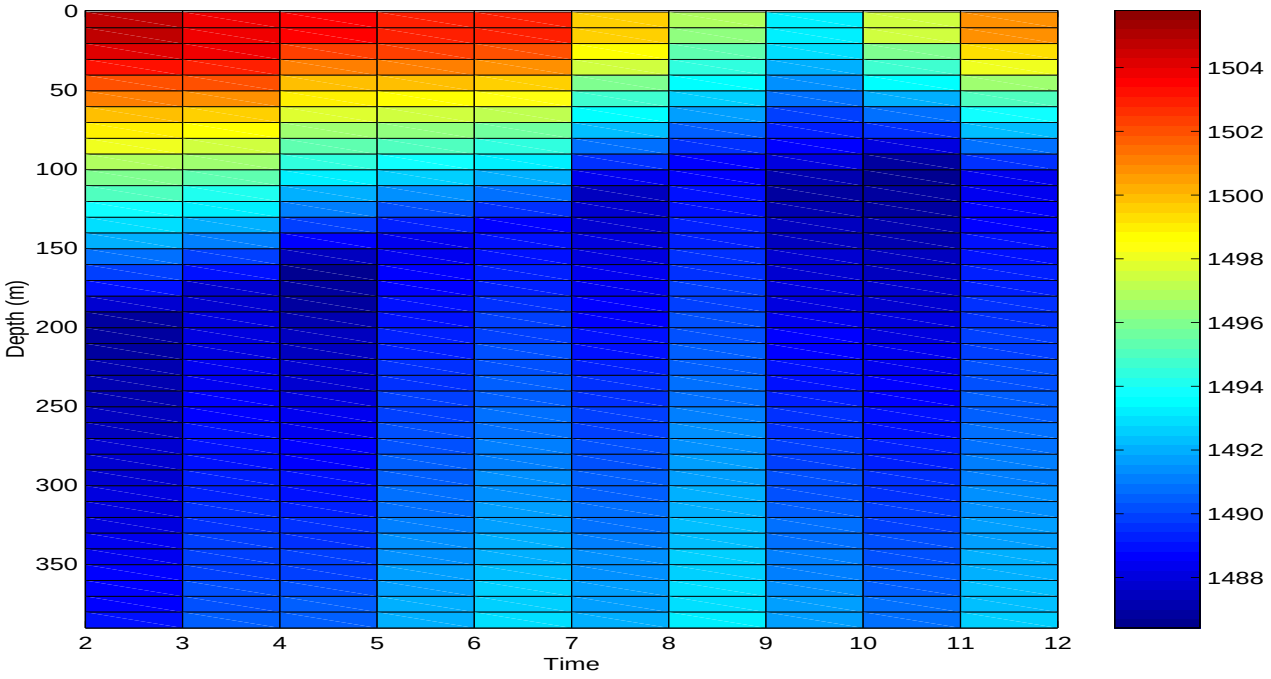

Figure 4.22: *Estimated sound-speed profiles in the middle cell for scenario 5, cell width 7 km, distance from source 11 km. The true profiles are given in fig. 4.2.*

Chapter 5

Conclusion

In this report, we investigated the performance of a MFI method based on a simplistic ocean model for upwelling detection and tracking. The problem consisted in estimating the sound-speed profile associated with the upwelling, its location and its width, as well as their variations in time. The challenge was to do so with a single pair of source-vertical array.

Simulation studies showed that the parameter estimates were rapidly and well determined in the ideal case where no source of mismatch was present. More than the width of the upwelling, it was its position relative to the array and source that had the most effect on the inversion results. With correlated noise in the data, the estimates were still well estimated for a 10 dB SNR but significantly degraded for 5 dB. Finally, the addition of transition cells in the true waveguide model increased the level of misfit. However, up to a cell width of 500 m, the parameter estimates were relatively good and it was possible to detect the upwelling.
A systematic study of the performance of the inversion for various properties of the upwelling and positions of the array and the source emphasized the dependence of the parameter estimates accuracy to all of these parameters. However in most cases, and despite the presence of noise, the upwelling was well visible.

The results obtained in the above simulations showed the feasibility of monitoring an upwelling with a single pair of source-array, even in non-ideal conditions. In the future, other important sources of mismatch such as more complex sound-speed profiles or inaccurate knowledge of the hydrophone position should be studied.

Bibliography

[1] W. Munk, P. Worcester, and C. Wunsch, *Ocean acoustic tomography.*, Cambridge Monographs on Mechanics, University Press, Cambridge, 1995.

[2] A. Tolstoy, O. Diachok and L.N. Frazer, "Acoustic tomography via matched field processing", J.Acoust.Soc.Am., **89**, pp 1119-1127, 1991.

[3] M.D. Collins and W.A. Kuperman, "Focalization: Environmental focusing and source localization", J.Acoust.Soc.Am., **90**, pp 1410-1421, 1991.

[4] C.M. Ferla, M.B. Porter and F.B Jensen, "C-SNAP: Coupled SACLANTCEN normal mode propagation loss model", Memorandum SM-274, SACLANTCEN Undersea Research Center, La Spezia, Italy, 1993.

[5] W.H. Press, B.P. Flannery, S.A. Teukolsky and W.T. Vetterling, *Numerical Recipes - The Art of Scientific Computing 2nd ed.*, Cambridge University Press, Cambridge, 1992.

[6] *Genetic algorithms in search, optimization and machine learning* Addison Welssey Publishing company, Reading, MA, 1989.

[7] V. Corré, "A two-stage matched-field tomography method for estimation of geoacoustic properties", Ph.D. thesis, University of Victoria, 2001.

[8] R.K. Dewey, J.N. Moun, C.A. Paulson, D.R. Caldwell and S.D. Pierce, "Structure and dynamics of a coastal filament", J.Geophys.Res., **96**(C8), pp 14885-14907, 1991.

Appendix A

Description of the files related to sound-speed estimation

This appendix provides the technical aspects of the inversions presented in the report. It intends to serve as a guideline for future users of the inversion method as well as to help in the access to the results shown above. Starting with an overview of the general organization of the files, the appendix continues by describing how to run an inversion. Finally and for future reference, a list of the files containing the results already obtained is given.

A.1 Content of the directory

All files related to this report are located in home/vcorre/mycsnap/. The mycsnap/ folder contains the following files and subfolders:

- sensi_vel_midgr/ : Contains the sensitivity results.
- sga_vel_midgr/ : Contains the inversion results. The conditions of inversions are listed in tabs. A.3 and A.4. The figures are in the ps/ subfolder.
- vel_mid_grad/ : Contains fortran library for the *csnap_velmid_gr* executable.
- *csnap.m* : A matlab routine which calls *csnap_velmid_gr*.
- *csnap_velmid_gr* : A fortran executable which combines C-SNAP and SGA to perform the inversion.
- *filament.txt* : Contains temperature and salinity measurements from a cold filament region. Serves as input file for *csnap.m*.
- *ind.dep2* : Derived from *filament.txt* (see *get_depth_fila.m*). Contains the two points which define the thermocline at each range. Serves as input file for *csnap.m*.
- *input* : Contains the input information about the waveguide and inversion parameters. Serves as input file for *csnap.m*. A description of this file is given in tabs. A.1 and A.2.

The main program is the fortran executable *csnap_velmid_gr* which performs the core inversion. This program requires two input files (*input_tmp* and *inp.vel*) that define the true environment properties and the inversion parameters. These two files are read in the *vel_mid_grad/csnap_velmid.f* routine which is the main fortran routine. From there, the pressure field is calculated for the true environment (*vel_mid_grad/make_true.f*) using a "plug-in" version of C-SNAP. For computational time issues, this version does not read or write any file. Once the true pressure field is calculated, the search for the minimum misfit is done using the SGA (*vel_mid_grad/vsga_digital.f*). The replica fields are also calculated with the same C-SNAP version. Different options are possible for calculating the misfit (see tabs. A.2). Finally, two outputs are generated: *log.out* (in *csnap_velmid.f*) and *out* (in *vsga_digital.f*). The first file is an ASCII file containing the set of parameters with minimum misfit. The second file is a binary file containing all the sets of parameters that were tested during the SGA inversion.

Note that *csnap_velmid_gr* program can also be used to calculate parameter sensitivity. In that case, there is an unique output file (*log.out*).

csnap_velmid_gr can be called directly at the Linux prompt. However for convenience, a Matlab routine *csnap.m* was developed to automate the editing of the input files, the inversions and the storage of the results. In addition, *csnap.m* can also be used to plot these results.

csnap.m works as follows. The routine reads *ind.dep2*, *filament.txt* and the user-defined *input* file. From the filament data, some profiles are chosen manually to define the true, time-dependent and range-dependent environment. According to the user choice (inside *csnap.m*), inversions are repeated over time loops and/or number of inversions per scenarios. After each inversion, the output files of *csnap_velmid_gr* are stored in the *sga_vel_midgr/* folder, as well as a copy of the *input* file to keep track of all inversion parameters. A sample of *csnap.m* describing the selection of the different options/parameters is shown in Appendix 2.

A.2 How to run a series of inversions?

To run one or several inversions, the user has first to edit the *input* file (see tabs. A.1 and A.2) to define the properties of the waveguide and inversion parameters. The next step is to select the sound-speed profiles of the true environment. This selection is done inside the *csnap.m* routine. Finally, when inversions are done, *csnap.m* can be used to read and plot the results. See Apppendix 2 and *csnap.m* for detailed explanations about the selection of sound-speed profiles and the description of the different plots available.

Table A.1: *Example of input file. Parameters with (*) are C-SNAP parameters for which more information can be obtained in the C-SNAP user guide [4]. Parameters with (**) are SGA parameters (see [7]).*

10	noise in db (if set to 99 then no noise)
437	if set to 1 then white noise; otherwise it feeds the random number generator to have correlated noise
0	if set to 1 then the bathymetry is unknown
0	if set to 1 then the sediment parameters are unknown
0	if set to 1 then the source depth is unknown
400.	water depth (m)
20.	sediment thickness (m)
1.4	sediment density (g/cm3)
2.	subbottom density (g/cm3)
1600.	P-wave velocity at top of sediment layer (m/s)
1.	P-wave velocity gradient in sediment layer (1/s)
1800.	P-wave velocity in subbottom (m/s)
0.1	P-wave attenuation in sediment layer (dB/λ)
0.5	P-wave attenuation in subbottom (dB/λ)
0	dummy
90.	source depth (m)
1	number of arrays (must be 1)
4	distance between receivers
33.5	array position (km)
50. 78. 146. 174.	depth (m) of shallowest and deepest receivers of first subarray and second subarray
0	dummy
2	number of frequencies (*)
250.1	minimum frequency (*)
349.1	maximum frequency (*)
8	number of FFT points (*)
250.5	lower frequency (*)
499.1	higher frequency (*)
0.0005	time sampling (*)
35	sga population (**)
10000.	maximum number of iterations (**)
0.85	mutation rate (**)
0.01	mutation rate decrease (**)
0.95	cross rate (**)
10.	number of iteration per DHS (**)
.25	increase rate number of iteration per DHS (**)
0.00000001	ftol (**)
0.000001	ptol (**)
2	cross-over (0:single point, 1:multi point, 2:double point) (**)
1	parent selection (0:random, 1:tournament) (**)
2	processor (1:pairwise, 2:incoherent bartlett, 3:coherent bartlett, 4:single frequency)

Table A.2: *Example of input file (end)*

10. 50.	search interval for sediment thickness (m)
1. 2.	search interval for sediment density (g/cm3)
0. 2.	search interval for sediment attenuation (dB/λ)
1590. 1650.	search interval for sediment velocity (m/s)
0. 2.	search interval for sediment velocity gradient (1/s)
1.5 2.5	search interval for subbottom density (g/cm3)
0. 2.	search interval for subbottom attenuation (dB/λ)
1700. 1850.	search interval for subbottom velocity (m/s)
394. 405.	search interval for water depth (m)
8	number of values per parameter for sensitivity computation
0	dummy
1480. 1510.	search interval for water sound speed (m/s)
2. 250.	search interval for depth points (m)
3 3	search interval for source depth $\pm Z_s$(m)
50.	max random variation of range limits in time (m)

A.3 List of inversion scenarios

Tabs. A.3 to A.5 list all the inversions presented in the report (figures or tables). Otherwise specified in the tables, the inversion parameters are those defined in Sec. 4.1. The output filenames (in sga_vel_midgr/) are coded according to the log.resX_TY formulation, where X is the scenario number and Y is the time window number. The *out* files were not saved.

Table A.3: *List of inversion scenarios*

X	$R_2 - R_1$	R_1	SNR	**trans**	R_a	Z_s	array
130	12	5	∞	0	33.5	90	50, 146
131	12	11	∞	0	33.5	90	50, 146
132	12	17	∞	0	33.5	90	50, 146
140	7	5	∞	0	33.5	90	50, 146
141	7	11	∞	0	33.5	90	50, 146
142	7	17	∞	0	33.5	90	50, 146
150	2	5	∞	0	33.5	90	50, 146
151	2	11	∞	0	33.5	90	50, 146
152	2	17	∞	0	33.5	90	50, 146
84	12	11	5	0	33.5	90	50, 146
9	10	10	∞	1000	33.5	90	50, 146
10	10.5	10.25	∞	750	33.5	90	50, 146
11	11	10.50	∞	500	33.5	90	50, 146
12	11.5	10.75	∞	250	33.5	90	50, 146
13	11.8	10.90	∞	100	33.5	90	50, 146

Table A.4: *List of inversion scenarios (continued)*

X	$R_2 - R_1$	R_1	SNR	trans	R_a	Z_s	array
30	12	5	10	0	33.5	90	50, 146
31	12	11	10	0	33.5	90	50, 146
32	12	17	10	0	33.5	90	50, 146
40	7	5	10	0	33.5	90	50, 146
41	7	11	10	0	33.5	90	50, 146
42	7	17	10	0	33.5	90	50, 146
50	2	5	10	0	33.5	90	50, 146
51	2	11	10	0	33.5	90	50, 146
52	2	17	10	0	33.5	90	50, 146
33	12	5	10	0	27.5	90	50, 146
34	12	11	10	0	27.5	90	50, 146
43	7	5	10	0	27.5	90	50, 146
44	7	11	10	0	27.5	90	50, 146
45	7	17	10	0	27.5	90	50, 146
53	2	5	10	0	27.5	90	50, 146
54	2	11	10	0	27.5	90	50, 146
55	2	17	10	0	27.5	90	50, 146
36	12	5	10	0	20.5	90	50, 146
46	7	5	10	0	20.5	90	50, 146
47	7	11	10	0	20.5	90	50, 146
56	2	5	10	0	20.5	90	50, 146
57	2	11	10	0	20.5	90	50, 146
58	2	17	10	0	20.5	90	50, 146
60	12	5	10	0	33.5	90	114, 146
61	12	11	10	0	33.5	90	114, 146
62	12	17	10	0	33.5	90	114, 146
63	7	5	10	0	33.5	90	114, 146
64	7	11	10	0	33.5	90	114, 146
65	7	17	10	0	33.5	90	114, 146
66	2	5	10	0	33.5	90	114, 146
67	2	11	10	0	33.5	90	114, 146
68	2	17	10	0	33.5	90	114, 146
70	12	5	10	0	33.5	90	50, 82
71	12	11	10	0	33.5	90	50, 82
72	12	17	10	0	33.5	90	50, 82
73	7	5	10	0	33.5	90	50, 82
74	7	11	10	0	33.5	90	50, 82
75	7	17	10	0	33.5	90	50, 82
76	2	5	10	0	33.5	90	50, 82
77	2	11	10	0	33.5	90	50, 82
78	2	17	10	0	33.5	90	50, 82

Table A.5: *List of inversion scenarios (end)*

X	$R_2 - R_1$	R_1	SNR	trans	R_a	Z_s	array
90	12	5	10	0	33.5	120	50, 146
91	12	11	10	0	33.5	120	50, 146
92	12	17	10	0	33.5	120	50, 146
93	7	5	10	0	33.5	120	50, 146
94	7	11	10	0	33.5	120	50, 146
95	7	17	10	0	33.5	120	50, 146
96	2	5	10	0	33.5	120	50, 146
97	2	11	10	0	33.5	120	50, 146
98	2	17	10	0	33.5	120	50, 146
100	12	5	10	0	33.5	70	50, 146
101	12	11	10	0	33.5	70	50, 146
102	12	17	10	0	33.5	70	50, 146
103	7	5	10	0	33.5	70	50, 146
104	7	11	10	0	33.5	70	50, 146
105	7	17	10	0	33.5	70	50, 146
106	2	5	10	0	33.5	70	50, 146
107	2	11	10	0	33.5	70	50, 146
108	2	17	10	0	33.5	70	50, 146

Appendix B

Sample of the csnap.m file

Note: each line starting with "%" is a comment.

```
% csnap.m


dis=[11., 23.];
% range limits (in km) of middle cell of true waveguide (R1 and R2 in fig. 2.1).
% if there are transitions cells, simply add the new ranges ex: dis=[11., 11.2, 22.8, 23.].

index_cell1=[50,50,50,50,50,50,50,50,50,50,50];
index_cell3=[50,50,50,50,50,50,50,50,50,50,50];
index_cell_int=[50,48,44,42,40,38,36,34,33,35,36];
% index_cell1, index_cell3 and index_cell_int contains the sound-speed profile index
% respectively for the first cell (where the source is), for the last cell (where the array is)
% and for the middle cell, for the different time windows.
% This example corresponds to a time-invariant profile in the first and last cells.
% In addition, these 2 cells have identical profiles here.
% The index (50) corresponds to the 50^th range profile of the real data
% i.e. the range variations of the measured temperature and salinity (in filament.txt)
% are transformed in time variations of the middle cell.

plo=0;
% If set to 1, plot inversion results or sensitivity.
% If set to 0, run the inversions or sensitivity calculation.

inv=1;
% If set to 1, run the inversions.
% If set to 0, do sensitivity calculation.

opt_dep=1;
% if set to 1 then depths are unknown during inversion.


opt_eps=0;
% if set to 1 then eps files are generated when a plot option is required.
```

```
nfile=300;        % index of the output filenames

premier=2;        % first time window to invert

ntime2=3;         % number of time windows to invert starting from premier

ninv=2;           % number of inversions per time window

% what to plot?
plo2=0;           % 1: plot population evolution for 1 inversion
plo3=0;           % 1: plot all tested model for 1 inversion
plo4=0;           % 1: plot results from multiple inversions and 1 time window
plo1=2;           % 1: plot true and final speed; 2: temperature
plo6=0;           % 1: plot misfit varying with time
plo7=0;           % 1: plot range limit varying with time
plo8=0;           % 1: plot final and true speed varying with range 2: temperature
```

With the options shown above, six inversions would be carried out (2 inversions $\times$ 3 time windows) and the output files would be:
log.res300_T2, *log.res300_T3*, *log.res300_T4*, (copy of *log.out*)
input300 (copy of *input*)
out300_T2_1, *out300_T2_2* (copy of *out* for the two inversions of the second time window)
out300_T3_1, *out300_T3_2* (copy of *out* for the two inversions of the third time window)
out300_T4_1, *out300_T4_2* (copy of *out* for the two inversions of the fourth time window).